CO_2 in the Atmosphere: Growth and Trends Since 1850 FREE

Michel Ramonet, Laboratoire des Sciences du Climat et de l'Environnement, Abhishek Chatterjee, Jet Propulsion Laboratory, Philippe Ciais, Laboratoire des Sciences du Climat et de l'Environnement, Ingeborg Levin, Universitaet Heidelberg, Mahesh Kumar Sha, Royal Belgian Institute for Space Aeronomy, Martin Steinbacher, Empa, Swiss Federal Laboratories for Materials Science and Technology, and Colm Sweeney, National Oceanic and Atmospheric Administration

https://doi.org/10.1093/acrefore/9780190228620.013.863

Published online: 21 June 2023

Summary

Very accurate long-term measurements of atmospheric CO_2 concentrationsbi are needed to understand the role of human activities on the greenhouse effect, as well as the interactions between anthropogenic emissions and the natural carbon cycle. Knowledge of the carbon cycle has been acquired through the development describes the development of atmospheric measurement networks and methods for measuring CO_2 in the atmosphere, including the measurement of CO_2 in air bubbles extracted from ice cores, the emergence of precise in situ measurements at the beginning of the 1960s, and the operational networks now deployed in certain parts of the world. The surface network of atmospheric stations where CO_2 is measured, either in air samples or by in situ instrumentation, made up of about 150 monitoring sites, supplemented by airborne measurements on board of research and commercial aircrafts, is coordinated by international projects aimed at guaranteeing a long-term measurement compatibility to within approximately 0.025‰ (0.1 ppm). This level of accuracy is necessary to characterize atmospheric signals such as the long-term trend, which has risen in 60 years from 1 to 2.2 ppm/year, but also the interannual, seasonal, and regional variations of CO_2. These atmospheric signals provide unique information about natural biogeochemical cycles and their current disturbance. The additional measurement of radiocarbon in atmospheric CO_2, as described in this article, also makes it possible to identify the contribution due to fossil fuel CO_2 emissions. The logistics and metrological requirements of in situ measurements mean that the monitoring network only covers the globe very incompletely—hence the importance of satellite observations, which have been developing strongly since their emergence in the early 2000s. Recent space-based CO_2 observations make it possible to measure the concentration of CO_2 averaged in the atmospheric column with global coverage under cloud-free conditions, providing millions of measurements each year, with a precision that can now reach 1 ppm, thus 10 times less than in situ instrumentation. Similar measurements of total CO_2 columns are also made by ground-based remote sensing instruments, at about 100 sites over the world. They provide important reference data to evaluate atmospheric CO_2 measurements from satellites and, in combination with in situ measurements of vertical profiles, provide a transfer standard between the satellite measurements and ground-based in situ networks.

This article provides an overview of CO_2 monitoring programs and what they tell about large-scale biogeochemical change. The perspectives for the development of CO_2 observations are important both for surface networks and for space-based observations, with the objective of moving toward the characterization of processes at increasingly fine spatial scales, in particular toward urban emissions.

Keywords: CO2, atmosphere, monitoring, isotope, satellite, gradients, trend

Subjects: Climate Systems and Climate Dynamics

Introduction

The precise and systematic monitoring of atmospheric carbon dioxide (CO_2) concentrations was initiated by C. D. Keeling at the end of the 1950s (Keeling, 1960; Keeling & Rakestraw, 1960), at the Mauna Loa Baseline Observatory, Hawaii (1958), and at the South Pole (1957).[1] The choice of these sites, very far from the emissions associated with human activities as well as from CO_2 exchanges between vegetation and the atmosphere, aimed to characterize CO_2 concentrations best representative of the Northern and Southern Hemispheres and their evolution in time. These two monitoring stations have operated almost without interruption since then and are the source of much of the knowledge on the global carbon cycle (Ciais et al., 2019; Fan et al., 1999; Keeling et al., 1996). Before the installation of innovative nondispersive infrared (NDIR) analyzers at these two stations for unprecedentedly precise (± 0.3‰) and continuous measurements, CO_2 concentration measurements were carried out by discrete sampling and offline chemical titration, starting from the late 19th century (Callendar, 1958; From & Keeling, 1986). Several research groups initiated air sampling programs, mainly in Europe but also in the Southern Hemisphere, between 1850 and 1940 (Baker, 2009; Fonselius, 1958). Various issues make it difficult to interpret the measurements by chemical titration. First, their questionable accuracy, estimated between 1% and 3%, is insufficient to distinguish, for example, spatial differences or seasonal variations. Second, observations often lack information on sampling and measurement protocols. Third, the sampling sites were often subject to strong local sources and sinks, whether of anthropogenic or biospheric origin. This type of local contamination, almost nonexistent at a site like the South Pole, can be effectively detected and filtered for a site like Mauna Loa (e.g., volcanic CO_2 emissions) thanks to continuous and precise measurement series but cannot be clearly identified in the time series of the discrete and discontinuous data. Therefore, samples from air trapped in Antarctic ice cores and firn are often used to reconstruct the atmospheric CO_2 concentrations for the pre-1958 period (Ahn et al., 2012; Berner et al., 1980; Etheridge et al., 1996; Petit & Raynaud, 2020; Raynaud et al., 2020; Rubino et al., 2019).

Over the past six decades, the CO_2 observation network has grown significantly, thanks in particular to the emergence of laser-optical sensors in the beginning of the current century (Werle et al., 2002) and analyzers based on cavity ring-down spectroscopy (CRDS) and cavity-enhanced absorption spectroscopy (CEAS; Baer et al., 2004; Crosson, 2008; Mazurenka et al., 2005). Technical development has significantly improved analyzer stability, as well as reduced the need for frequent calibrations and in-house development by scientific users. By 2010, such analyzers were widely available for CO_2 measurements in observatories (Rella et al., 2013) and on-board aircraft (Chen et al., 2010; Karion et al., 2013). The increasing number of sites and methods for monitoring CO_2 in the atmosphere helps to improve the knowledge of the exchange fluxes of this gas at increasingly fine spatial scales. To fulfill such objectives, the Global Atmosphere Watch (GAW) program under the umbrella of the World Meteorological Organization (WMO) coordinates a global network of 184 (World Meteorological Organization [WMO], 2022) high-precision atmospheric CO_2 ground-based in situ observations (WMO, 2021). The network

compatibility target for CO_2 measurements is ± 0.1 moles CO_2 per mol of air (ppm) for the Northern Hemisphere (i.e., on the order of 0.25‰ of typical ambient levels). For the Southern Hemisphere, the target is even more demanding, set to ± 0.05 ppm (WMO/IAEA, 2020). Data are publicly available in GAW's World Data Centre for Greenhouse Gases (WDCGG *<https://gaw.kishou.go.jp>*); hosted by the Japanese Meteorological Agency. Compilations are published annually in the WDCGG Summary Reports (World Data Centre for Greenhouse Gases, 2021). The ambitious compatibility requirement for a global network, and to maintain this over a time period of several decades, is justified by the amplitude of the atmospheric signals and gradients to be characterized over time and spaces. In parallel to CO_2 concentration measurements, monitoring of stable isotopes (^{13}C, ^{18}O) and radiocarbon (^{14}C) in CO_2 is also fundamental in disentangling the different CO_2 source and sink contributions in global and regional concentration signals. In addition to surface observations, the development of vertical/total column measurements in the troposphere and the stratosphere is essential to characterize the dispersion of CO_2 within the atmosphere and to verify the capacities of atmospheric transport models to represent this process (Stephens et al., 2007). Such measurements, either airborne onboard commercial aircraft (Filges, 2020; Sawa et al., 2015; Umezawa et al., 2018, 2020) or research airplanes (Baier et al., 2020; Long et al., 2021; Sweeney et al., 2020), by in situ sampling and offline analysis or by ground-based remote sensing allow making the link between precise and calibrated surface measurements and total column CO_2 measurements observed from satellites. In Sections "Representativeness of the Surface Monitoring Sites," "Spatial Variations of CO_2 Observed From the Background Surface Network," "Airborne Measurements," "Satellite Observations of CO_2 Total Columns," "Ground-Based Remote Sensing Observations of Atmospheric CO_2," the different CO_2 observation networks that are now in place are described, as well as the signals observed by these networks. The different types of measurement considered in this work are represented schematically in figure 1.

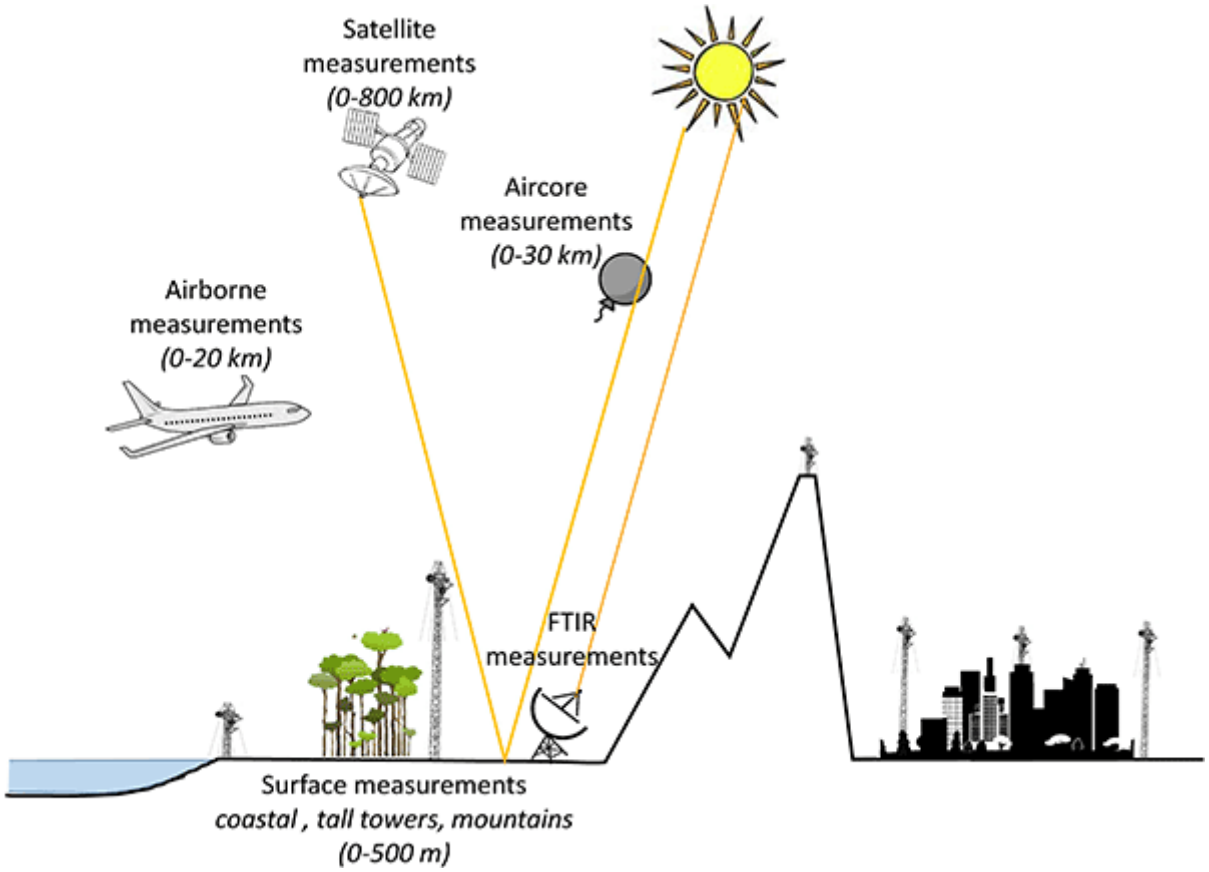

Figure 1. Schematic of the in situ and remote sensing CO_2 measurement across the atmospheric range covered by the various measurement techniques (numbers in brackets in m and km above ground).

Source: Image generated by authors.

Representativeness of the Surface Monitoring Sites

The CO_2 concentrations measured at a given location vary continuously under the influence of surface processes and atmospheric transport. Due to the long lifetime of CO_2, recorded data at a given point are influenced by contributions from local, regional, and larger-scale sources (emissions to the atmosphere) and sinks (uptake from the atmosphere). The relative contributions of these processes occurring at different scales to the atmospheric concentration of CO_2 depend on the intensity of both atmospheric mixing and source/sink strengths. Lateral advection and vertical transport favor the mixing of those contributions all together, while low wind speeds tend to increase the signals of local processes. Moreover, the height and stability (by modulating the vertical diffusion rate) of the planetary boundary layer also modulates the observed strength of the CO_2 enhancement per unit of surface emission (Denning et al., 1995; Okada et al., 2012). Consequently, observations will usually contain a mix of signals due to different processes at different scales in time and space. It will require atmospheric transport modeling to decompose the different signals to be able to compare this with the observational truth and improve the uncertainties in the process information. Traditionally, the Global Atmosphere Watch global network consists of sites in remote locations providing information on

carbon exchanges at relatively large spatial scales. This was particularly true in the early decades of the deployment of CO_2 measurement stations, where each station was seen to be representative, for example, of the latitudinal band in which it is located, assuming that longitudinal transport is fast compared to the time scale considered (e.g., monthly; Tans et al., 1990). To avoid as much as possible the influence of local anthropogenic and biospheric sources, ubiquitous in the continental boundary layer, the strategy has been to install stations in deserts or drylands, on remote islands or coastal sites, or on top of mountains with a strict selection of data to remove local effects (e.g., upslope winds) or to use tall towers or aircraft that allow sampling in the middle of the boundary layer and above. The scientific objectives for this station location strategy were to determine the global trends, the meridional distribution of CO_2, and the air–surface exchange with the ocean and terrestrial biosphere at very large scale (Ciais et al., 1995).

The first atmospheric modeling studies (Heimann et al., 1986; Keeling et al., 1989; Tans et al., 1989, 1990), which inferred the distribution of surface CO_2 fluxes in the late 1980s and early 1990s, primarily exploited the observed gradients of CO_2 in latitude to deduce latitudinal mean fluxes at monthly or annual time scale. Generally, CO_2 gradients in longitude at these time scales are small because atmospheric circulation is favoring transport and mixing from West to East rather than from North to South, especially in the middle and high latitudes. Nevertheless, Fan et al. (1998) were the first to exploit longitudinal CO_2 gradients—namely, the small negative difference of CO_2 between upwind stations in Pacific Ocean and downwind stations around North America. They concluded that the vegetation in North America was a huge sink of carbon (Fan et al., 1998).

During the past two decades, extended networks have been developed, mostly in North America (Unites States and Canada; Andrews et al., 2014; Sweeney et al., 2015); in western Europe, where the emergence of the European Integrated Carbon Observation System research infrastructure since 2015 has led to the establishment of a dense and standardized network (Heiskanen et al., 2022; Palmer et al., 2018); and in northeast Asia, aiming to let models quantify CO_2 fluxes at continental and subcontinental scale (Baker et al., 2006; Broquet et al., 2013; Thompson et al., 2016). These networks will allow the study of the exchange fluxes and their influence on atmospheric concentrations also at smaller scales in time and space, which poses an equivalent challenge to the accuracy of the transport modeling at the appropriate scales. Eastern Europe and Russia remain very poorly sampled, despite their large vegetated areas, which play an important role in the carbon cycle. Most of the long-term measurements in Russia come from early and sustained efforts from the observation program of the National Institute for Environmental Studies in Japan (Belikov et al., 2019; Saeki et al., 2013), and since 2006, continuous atmospheric greenhouse gases measurements have been conducted by the Max Planck Institute for Biogeochemistry in Jena, Germany, at a custom-built 300-m tall tower in Zotino (Kozlova et al., 2008). The development of regional networks has led to the installation of more and more stations in the heart of continents to follow the evolution of air masses as they become exposed to carbon exchanges with urbanized areas and terrestrial ecosystems. Due to the high variability of these sources and sinks of CO_2, atmospheric concentrations at such stations exhibit significantly greater variability than oceanic and coastal stations (Levin et al., 1995).

Figure 2 represents the variations of CO_2 observed during 1 year (2018) at three typical measuring stations of the global network: Amsterdam Island, background station in the Southern Hemisphere; Puy de Dôme mountain station in central France; and Trainou, a rural station located 100 km south of Paris. The first two stations are representative of ocean and continental background stations, while the Trainou tower is in a rural environment but impacted by regional processes. In order to limit the influence of local emissions, a high telecommunications tower is used at Trainou, a strategy now common for the continental stations (Andrews et al., 2014; Bakwin et al., 1998; Kozlova et al., 2008; Schmidt et al., 2014; Vermeulen et al., 2011), which has the advantage of offering CO_2 measurements on flat terrains that are easier to represent with atmospheric transport models than more complex terrain like mountain stations. In all cases, a data selection procedure is applied to select conditions in which the transport errors in atmospheric transport models are thought to be minimal and most representative for the point sampling by identifying the periods of low local influence. This is a common strategy often applied to time series also from remote locations to maximize the spatial representativeness of the data. Many different approaches have been developed in the past (Chambers et al., 2016; Levin et al., 1995; Ramonet & Monfray, 1996; Ruckstuhl et al., 2012; Thoning et al., 1989). On the three sites presented in figure 2, the data least influenced by local emissions are shown in red. The applied approaches were station specific: For the Trainou plain station, afternoon data (12:00–17:00 hr local time) are selected when the air masses are well mixed; for the Puy de Dôme mountain station, on the contrary, nighttime data (20:00–05:00 hr local time) are selected in order to avoid the periods of uplifting air, which occurs during the day (Lopez et al., 2015). An additional criterion is applied to filter out hours with a standard deviation of 1-min values greater than 0.5 ppm. Finally, at Amsterdam Island, a criterion based on local wind speed and direction is used in order to isolate the air masses, which have been in contact with the small island. A common feature to the three stations is the increase in variability during the summer period, indicating very clearly the influence of biospheric fluxes. Even on Amsterdam Island, a small island in the middle of the Indian Ocean, diurnal cycles are observed between November and March during the austral summer. However, the amplitude of the diurnal variations is extremely variable depending on the type of station (figure 3). At Amsterdam Island, the diurnal variability is on the order of ± 1 ppm and insignificant when only marine air masses are considered. For a mountain station like Puy de Dôme, the short-term variability is on the order of ± 5 ppm in summer and ± 2 ppm in winter, with no significant differences between selected and nonselected data sets. At the rural station Trainou, the variability observed at 180 m above the ground is of the same order as at Puy de Dôme, but at air intake locations closer to the surface, variations increase by an order of magnitude. In June, the nighttime values at 5 m above the ground are on average 50 ppm higher than the concentration observed at noon due to the net flux of CO_2 from plant and soil respiration. This high variability of CO_2 concentrations in continental environment illustrates the importance of the sampling strategy but also the difficulty for atmospheric transport models to correctly represent such differences on small scales of time and space. As the models have difficulties to reproduce such strong variability, studies often use only the concentrations of CO_2 selected as representative of large spatial scales (i.e., the selected data in figure 2). It may, however, be noted that measurements of boundary layer height or vertical gradients of

concentrations and meteorological conditions can be used to better identify well-mixed conditions in the boundary layer based on objective criteria instead of fixed and rigid patterns based on the time of day.

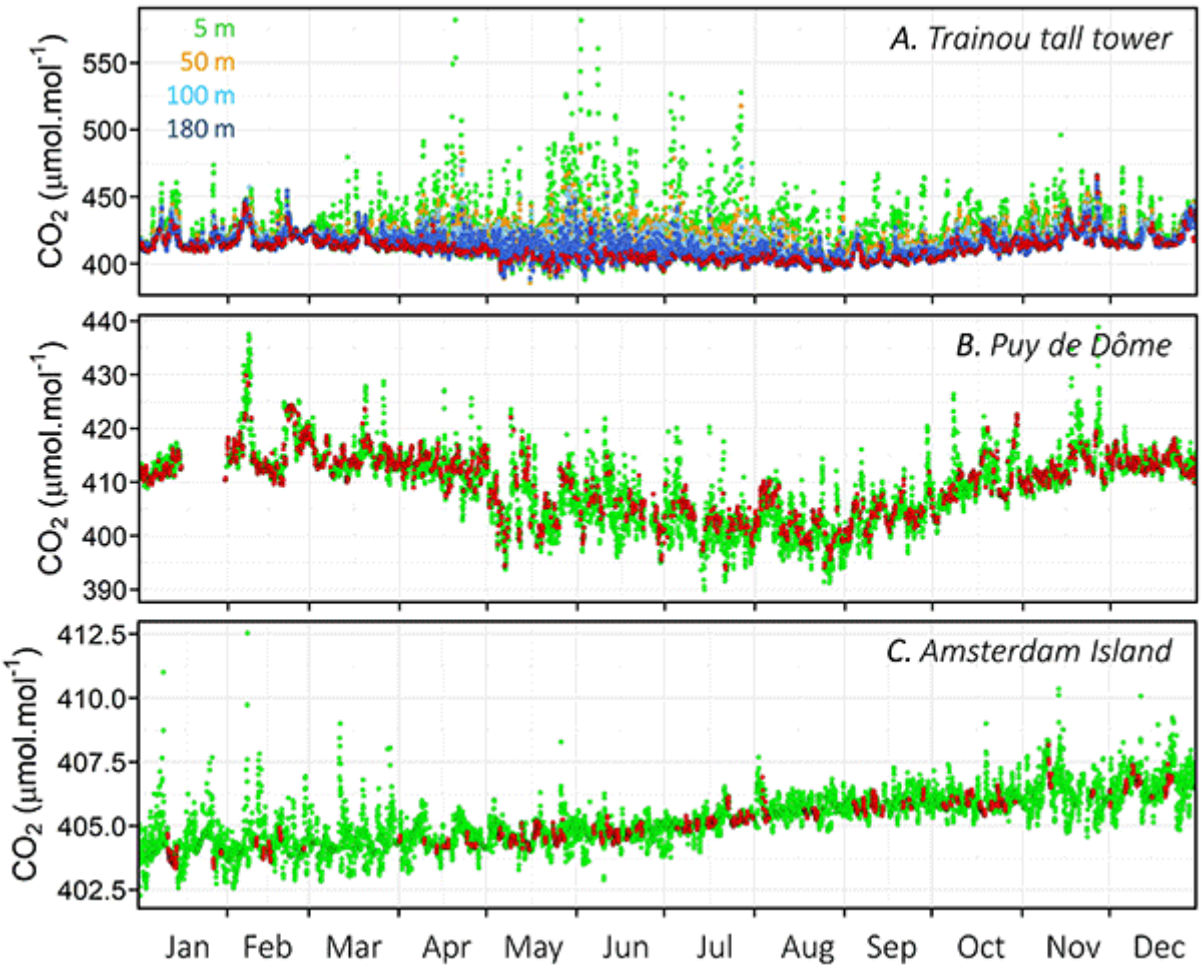

Figure 2. Hourly mean CO_2 concentrations observed in 2018 at (A) Trainou tall tower (with four sampling levels from 5 to 180 m above the ground), (B) Puy de Dôme, and (C) Amsterdam Island. Red dots are considered as data with lowest local influence. Please take note of the different y-axis scales for the different panels.

Source: Image generated by authors.

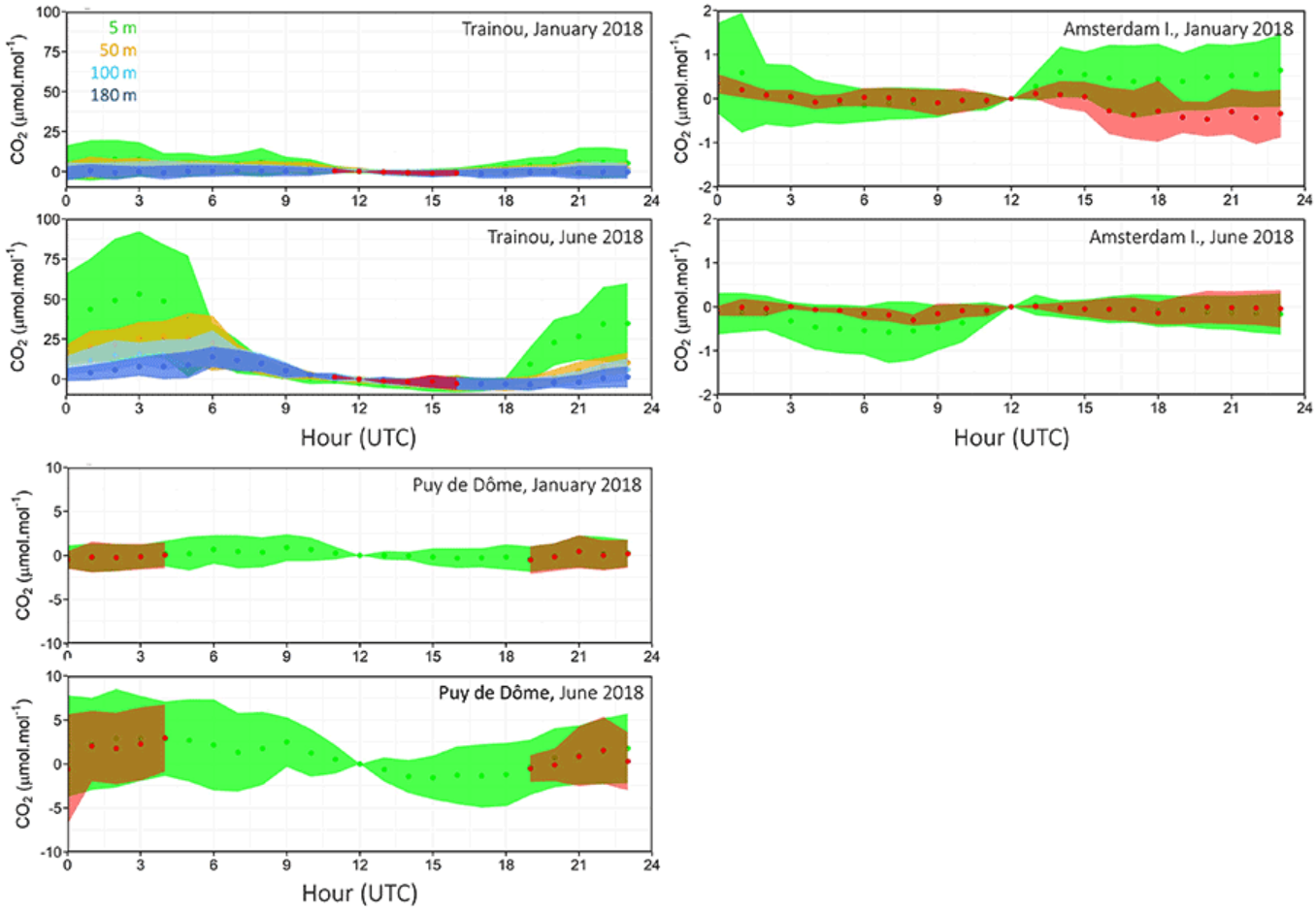

Figure 3. Mean CO_2 differences with respect to the value observed at 12-hr UTC. Red points and curves correspond to the data selected as representative of large-scale processes. For Trainou tall tower, the differences are calculated relative to the 12-hr UTC value observed at 180 m above the ground. Shaded areas represent the standard deviation over the month. Please note the different scales of the y-axes.

Source: Image generated by authors.

Spatial Variations of CO_2 Observed From the Background Surface Network

To date, 134 stations engaged in long-term CO_2 monitoring have been identified (Cox et al., 2021; ICOS-RI, 2020; Ramonet et al., 2020), without considering the stations located in urban areas, the number of which has increased sharply in recent years (figure 4). In this analysis, only the stations present in the World Data Centre for Greenhouse Gases, the Observation Package (OBSPACK-Globalview), and ICOS data portals were considered, and for all time series, a data selection based on the time of the day was applied. Among this network, 26 sites can be considered as mountain stations (located at an altitude of at least 1,000 m a.s.l.) and 48 as high towers (higher than 50 m). 33 stations performing regular sampling of air in flasks from the collaborative network of the Earth System Research Laboratories, National Oceanic and Atmospheric Administration (NOAA/ESRL <https://gml.noaa.gov/ccgg/flask.html>)were also taken

into account. All the samples are analyzed in a central measurement laboratory to maximize compatibility. Flask sampling and central offline analysis enable measurements in regions where local expertise and facilities do not allow for sufficiently precise and accurate in situ measurements. Figure 4 illustrates the abovementioned heterogeneity of the spatial coverage of observations. The four panels in figure 4 showing the CO_2 differences (after data selection for large-scale representativeness) compared to Mauna Loa, each for a selected month in 2018, provide a good overview of the seasonal consistency with which CO_2 varies at the Earth's surface. For Mauna Loa, the measurements selected as representative of background conditions, following the procedure explained in detail by the NOAA Global Monitoring Laboratory *<https://gml.noaa.gov/>*, represent on average 38% of the data. The variability over the seasonal cycle in the Southern Hemisphere remains quite small, with values lower than Mauna Loa by −2 to −6 ppm in February and May and within ± 2 ppm in August and November. Due to the larger land masses in the Northern Hemisphere, the seasonal cycle of CO_2 gradients is much more pronounced. During some winter months (February and November), terrestrial sites in the Northern Hemisphere are higher by +2 to +15 ppm compared to Mauna Loa. This corresponds to the period when the vegetation covering the Northern Hemisphere continents is a net source of CO_2 in addition to anthropogenic emissions. In May, lower values of a few ppm can be observed on the European continent, due to carbon uptake by plants, but most North American and Asian stations still show concentrations at least equal to Mauna Loa. In August, most North Hemisphere mainland stations are below Mauna Loa, with lower values in northern Europe compared to southern Europe and much higher minima at several stations in North America. Few stations in Asia still have higher CO_2 concentrations in spring and summer, indicating that for those stations, the influence of urban emissions is constantly exceeding the signal of the carbon uptake by the vegetation. Figure 5 summarizes the monthly CO_2 gradients observed in 2018 for all the stations, color-coded according to their latitude. The homogeneity is particularly striking among the stations of the Southern Hemisphere, with CO_2 lower than at Mauna Loa by up to 5 ppm approximately during austral summer/autumn. Overall, most of the observed CO_2 in the Northern Hemisphere remains within ± 15 ppm compared to Mauna Loa.

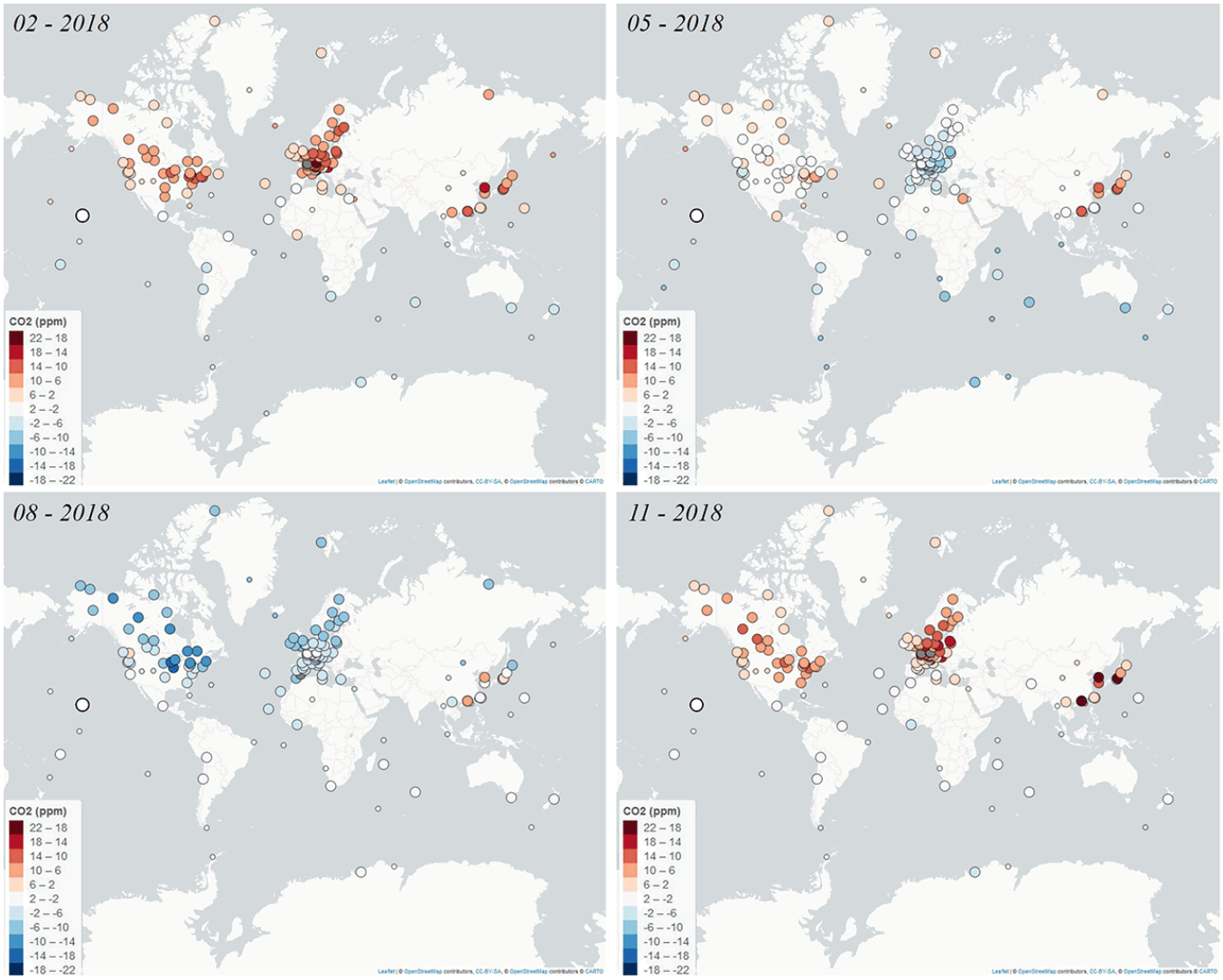

Figure 4. Monthly means of CO_2 differences in February, May, August, and November 2018 to Mauna Loa observatory (shown as a larger circle in the Pacific). Smaller circles represent the flask sampling sites, whereas the larger circles indicate the continuous monitoring sites. Stations located in urban areas are not considered, and data are selected to be representative of large-scale signals as used in atmospheric inversions.

Source: Image generated by authors.

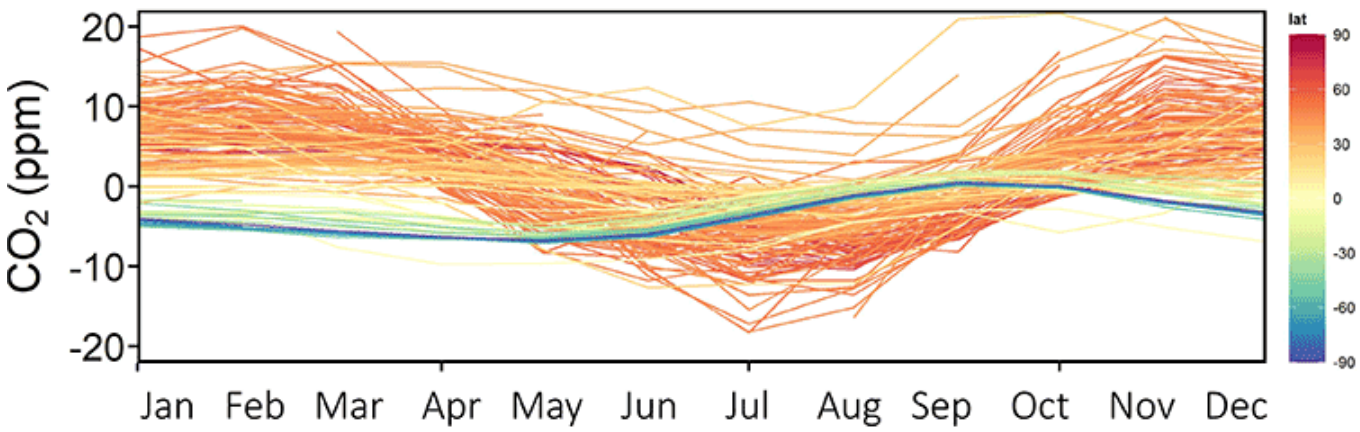

Figure 5. Monthly means of CO_2 differences in 2018 to Mauna Loa observatory. Each site is represented with a colored line corresponding to its latitude.

Source: Image generated by authors.

Airborne Measurements

With the increasing input of fossil fuels into the atmosphere since the Industrial Revolution, the vertical gradient of CO_2 in the atmosphere is also continually becoming more negative (concentration decreasing with altitude) with time. However, this mean vertical gradient is subtle compared to the gradients that can be observed throughout the vertical column on any given day due to variability in sources and sinks as well as transport on diurnal, seasonal, and annual time periods. Balloon and aircraft-based platforms are essential for providing a detailed picture of the vertical gradients that exist from the surface through the troposphere and stratosphere. These gradients, in turn, can provide a valuable constraint on the understanding of land and ocean sources and sinks (Gatti et al., 2010; Long et al., 2021; Stephens et al., 2007), as well as provide a valuable tool for evaluating and understanding large-scale vertical and horizontal transport (Hall et al., 1999). These measured gradients also play a critical role evaluating and understanding satellite retrievals, ground-based total column retrievals, and model simulations of CO_2. Once CO_2 has been released into the atmosphere through land and ocean fluxes, there are besides dispersion only few processes that significantly change the CO_2 concentration above the ground, except for oxidation of hydrocarbons and photodissociation at altitudes of 80 km. From this perspective, the vertical gradients of CO_2 preserve a record, which reflects the integrated change in CO_2 mole fraction of that air mass when it was last in contact with the ground.

Starting from the surface, where sources and sinks have direct influence on the atmospheric concentration (figure 6), it is possible to see during daytime and in absence of strong subsidence due to high-pressure systems a relatively homogeneous layer of CO_2 that extends to the top of the boundary layer due to vertical mixing driven by latent and sensible heat from land and ocean surfaces through surface warming by solar radiation and turbulence. The result of this turbulent mixing in the boundary layer is an almost constant mole fraction of CO_2 with altitudes to as high as 1,000–3,000 m above ground level, consistent with water vapor and potential temperature during the day. At night, a shutdown in the vertical mixing will result in an enhancement in the vertical gradient from ground level as emissions are trapped in the layers below the maximum mixing height of the previous day. At any given time, the mole fraction of CO_2 in the atmospheric column will reflect the cumulative input/removal of CO_2 over multiple days, and assuming significant horizontal transport, the net change in mole fraction will reflect the source/sink influence of large areas upwind of a given profile. Above the boundary layer, a relatively stable residual layer is often identified, which is the result of a previous diurnal cycle and reflects the influence of upwind surface processes experienced the day before as the air mass was then in the boundary layer. Above the residual layer is a middle and upper troposphere region where gradients are driven by wind shear, large-scale atmospheric overturning, and smaller-scale turbulence as well as faster frontal convergence. These processes result in the propagation of the boundary layer signal up to the tropopause on a time scale from day to month.

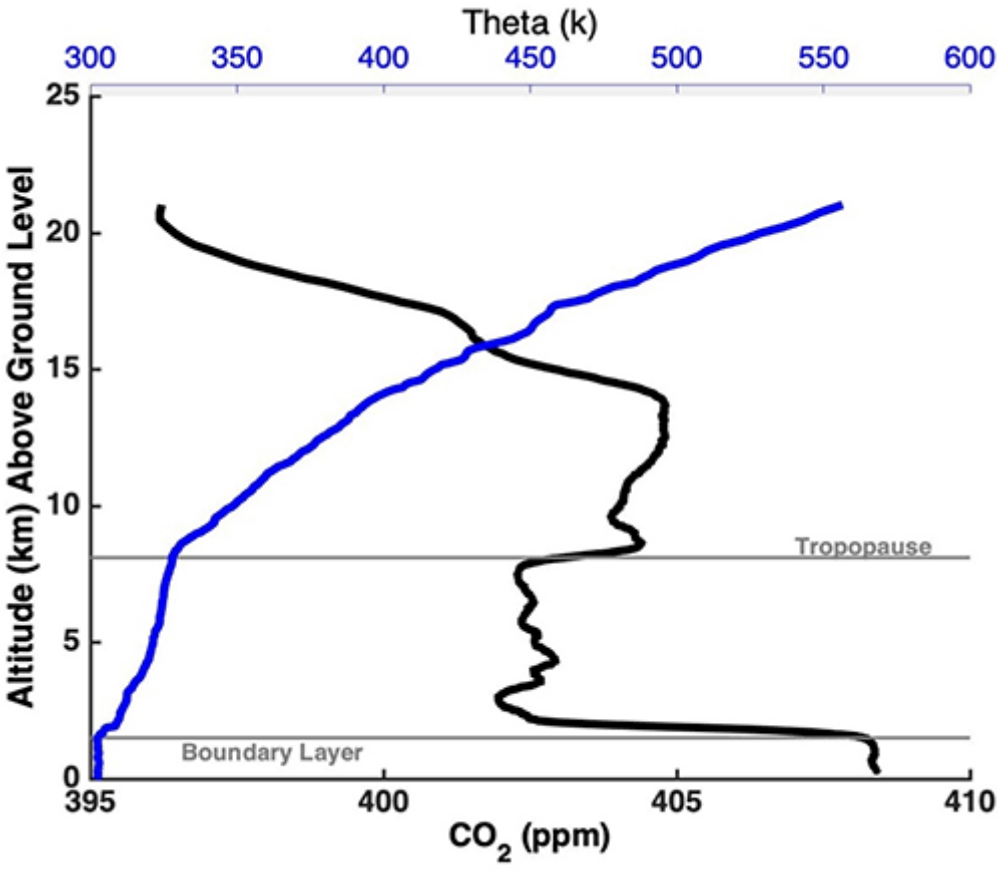

Figure 6. Potential temperature (theta) and CO_2 profile from AirCore flight on September 26, 2017, from Boulder, Colorado.

Source: Image generated by authors.

The vertical gradient of CO_2 in the stratosphere (figure 6) is largely reflecting slow vertical and horizontal mixing in the stratosphere and, to a lesser extent, input of air into the stratosphere from the troposphere. The main driver of this input into the stratosphere is predominately from the tropics through the Brewer–Dobson circulation (Butchart, 2014). With the annual rise of atmospheric CO_2 in the troposphere, a vertical gradient in the stratosphere is created, which reflects both the overturning rate of the stratosphere (Schmidt & Khedim, 1991) and mixing with the mesosphere, where CO_2 is eventually destroyed (Kaufmann et al., 2002).

The History of Airborne CO_2 Measurements

Measurements of CO_2 vertical profiles have been recorded as far back as 1874 (Tissandier, 1874), but it was not until the late 1950s that flask measurements from aircraft and balloons were considered robust enough to capture trends and vertical gradients that are globally significant (Bischof, 1962; Keeling et al., 1968). As early as 1957, a reproducibility of 0.2 ppm has been reported for aircraft samples taken from a variety of aircraft platforms, including commercial aircraft (Bischof, 1970; Bischof & Bolin, 1966; Bolin & Bischof, 1970; Keeling et al., 1968). Likewise, it was not until the mid-1990s that in situ measurements on aircraft and balloons had

reproducibility at levels of the 0.5‰ required by the World Meteorological Organization for such measurements (WMO/IAEA, 2020; Wofsy et al., 1988). Until then, most suitable aircraft measurements were made using flask samples. However, interest peaked for making in situ CO_2 measurements in the upper troposphere and stratosphere using high-altitude aircraft and large-balloon platforms, which motivated the development of CO_2 measurements that were stable enough to enable globally significant processes in the carbon cycle to be resolved (Anderson et al., 1993; Boering et al., 1994; Levin et al., 2002). In 1993, a multi-institutional collaboration with Japanese Airlines (JAL) was created to make regular flights throughout the western Pacific. Two years later, the National Ocean and Atmospheric Administration started a small aircraft network of regular profiles that expanded to 23 sites in North America and Rarotonga (Sweeney et al., 2015). Similarly, a European effort launched the projects called EuroSiberian-Carbonflux and TCOS-Siberia, which featured four sites in western Europe and Siberia starting in 1998 and lasting until 2005, when flask samples and in situ measurements were performed at 2- to 3-week intervals to 3,000 m a.s.l. (Levin et al., 2002; Ramonet et al., 2002). By 2005, researchers had improved the in situ analyzers for CO_2 to the point that JAL began making continuous measurements of CO_2 on commercial aircraft (Machida et al., 2008; Matsueda et al., 2008) with regular flights from Japan to Australia, Europe, Asia, Hawaii, and North America, providing large spatial data coverage, particularly in the Northern Hemisphere. In addition, the ease of deploying optical laser spectrometers has enabled deployments on many small planes for different applications like the study of distributed point source emissions from oil and gas to urban regions (Karion et al., 2015; Schwietzke et al., 2019, and references therein). Since 2020, cavity ringdown instrumentation has been deployed on European commercial aircraft programs such as IAGOS <*http://www.iagos.org/*> and CARIBIC <*http://www.caribic-atmospheric.com/*>, focused on long-haul flights from Europe to Asia, Africa, and North America (Filges et al., 2015; Schuck et al., 2009).

The development of optical instruments has made it possible to measure small-volume samples, particularly AirCores (Karion et al., 2010). Unlike a single flask, the AirCore allows a continuum of samples to be sampled over the atmospheric column using a long stainless steel tube (~100 m), transported by balloon to altitudes up to 30 km. The vertical profiles thus obtained have a vertical resolution of the order of 75 m in the boundary layer of the atmosphere and a few hundred meters in the stratosphere (Baier et al., 2023). AirCores are the only method capable of providing relatively inexpensive vertical calibrated CO_2 profiles from the ground to the stratosphere. They constitute an increasingly essential source of data for the validation of remote sensing measurements from the ground, or by satellite, and atmospheric transport models (Schneider et al., 2022; Sha et al., 2020; Tu et al., 2020; Yi et al., 2019). These vertical profiles calibrated by the international reference scale make it possible to establish a link between surface, airborne, and remote sensing measurements (Rastogi et al., 2021).

Uses of the Atmospheric Gradient of CO_2

CO_2 vertical gradients measured by aircraft and balloons provide a strong constraint on the underlying air–land and air–sea sources and sinks, as well as a direct measure of the fidelity of remotely sensed ground-based and satellite retrievals and model simulations, which may lack

information about transport processes that are critical to understand underlying fluxes of CO_2 into the atmosphere (Fung et al., 1983; Stephens et al., 2007; Tans et al., 1990). The information content of aircraft and balloon profiles falls into three broad categories: (a) boundary layer processes, (b) tropospheric gradients, and (c) stratospheric gradients.

While ground-based in situ CO_2 observations can provide a near-continuous observation of processes in the atmospheric boundary layer, some important shortcomings require a higher than available number of ground sites or accurate transport modeling to properly interpret these data. The biggest shortcoming of a ground-based in situ observation is generally the lack of knowledge about the boundary layer height. The aircraft profile can provide a direct measure of this, as shown in figure 6, where the CO_2 mole fraction is constant up to about 2 km height, indicating mixing extent of the boundary layer during the time of measurement. To infer a flux from a ground-based sensor, an estimate of the boundary layer thickness is required, and uncertainty in this layer height represents a significant source of error.

Similarly, above the boundary layer, wind shear often induces gradients that represent downstream fluxes that enable the vertical profile to provide information that would require many ground-based observations to capture (Hooghiem et al., 2020). In many studies, aircraft measurements above the boundary layer have been used to understand the background mole fraction of CO_2 before that air mass was affected by a surface flux (Gatti et al., 2021; Klausner et al., 2020).

Satellite Observations of CO_2 Total Columns

The background ground-based greenhouse gas monitoring network has been essential in establishing long-term trends and in providing important information about the global carbon cycle. However, it is not sufficient for quantifying sources and sinks at a local to regional scale all over the world and/or designed to quantify emissions from large point sources, such as cities or power plants. One way to expand the spatial and temporal coverage is to acquire global measurements at high spatial resolution from space (Chevallier et al., 2007; Eldering et al., 2017; Houweling et al., 2004; Hungershoefer et al., 2010; O'Brien & Rayner, 2002; Rayner & O'Brien, 2001). The first steps toward space-based remote sensing measurements of CO_2 were achieved using spectrometers that viewed the Earth's thermal emission or reflected sunlight. The first space-based sensor to use this approach was the European SCanning Imaging Absorption spectroMeter for Atmospheric CartograpHY (SCIAMACHY) onboard the European Space Agency (ESA) Environmental Satellite (ENVISAT), which operated from 2002 to 2012 (Bovensmann et al., 1999). Alongside NASA's Atmospheric Infrared Sounder on the Aqua satellite and ESA's Infrared Atmospheric Sounding Interferometer on the MetOp series of polar orbiting satellites, measurements are routinely acquired within atmospheric CO_2 bands, where CO_2 absorbs and emits thermal radiation. All three of these early multipurpose instruments had relatively coarse spectral resolution and large measurement footprints that limited their spatial resolution, as well as the precision and accuracy of CO_2 retrievals, typically yielding CO_2 mixing ratios with

accuracies of ~1% at altitudes in the middle troposphere (~5 km) but having little or no sensitivity near the surface (Chevallier et al., 2009). However, these were critical in demonstrating the feasibility of space-based spectrometers to address questions about atmospheric composition.

Since 2009, two satellite missions have been developed specifically for measuring atmospheric CO_2 using higher-resolution passive spectrometers. The Japanese Greenhouse gas Observing Satellite (GOSAT), launched in January 2009, flies in a 666-km altitude, sun-synchronous orbit with 3-day ground track repeat cycle. Its Thermal And Near infrared Sensor for carbon Observation (TANSO) Fourier Transform Spectrometer (FTS) has returned high-resolution spectra of reflected sunlight in the CO_2 bands near 1.57, 1.61, and 2.06 μm since April 2009 (figure 7). Several research groups across the globe are using these spectra to estimate column-averaged dry-air mole fractions of carbon dioxide (XCO_2) using various retrieval algorithms (Inoue et al., 2013; Noël et al., 2021; O'Dell et al., 2012; Yoshida et al., 2012). Observational biases and random errors have been gradually reduced that are typically less than 0.5% on regional scales over much of the Earth. These XCO_2 retrievals from GOSAT TANSO-FTS are being used in flux inversion models to improve our understanding of CO_2 sources and sinks in data-poor regions, such as tropical Africa and central Asia (Basu et al., 2013; Guerlet et al., 2013; Maksyutov et al., 2013).

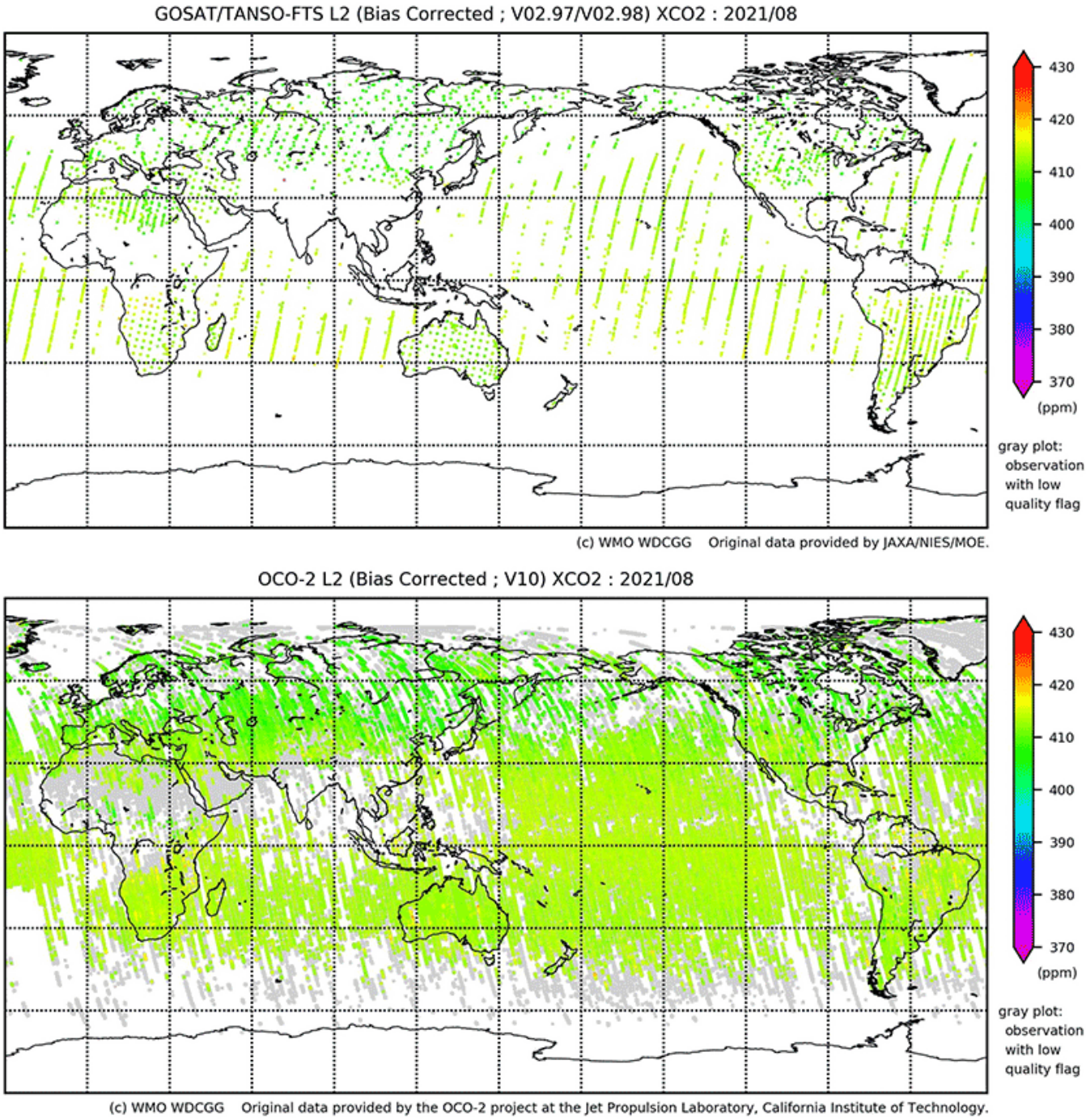

Figure 7. Monthly maps of XCO_2 estimates derived from (A) GOSAT and (B) OCO-2 measurements for August 2021. For both satellite products, the coverage at high latitudes varies with the availability of sunlight; however, thick clouds and aerosols limit the coverage.

Source: Image Credit: World Data Center for Greenhouse Gases <https://gaw.kishou.go.jp/satellite/>.

Furthermore, extending the space-based CO_2 observation program, NASA's Orbiting Carbon Observatory–2 (OCO-2) mission was launched during July 2014. OCO-2 mission uses optical spectrometers with higher-sensitivity detectors, and it views the Earth in smaller footprints. OCO-2 returns about three million XCO_2 estimates over the sunlit hemisphere each month with

single sounding random errors of ~0.5 ppm and accuracies of ~1 ppm (Müller et al., 2021; O'Dell et al., 2018; Wunch et al., 2017). OCO-2 flies at the head of the 705-km Afternoon Constellation ("A-Train"), in a sun-synchronous orbit, with a 1:30 p.m. equatorial crossing time and a 16-day repeat cycle (Crisp et al., 2004; figure 7). To yield more useful data in partially cloudy regions, the surface footprint of each OCO-2 sounding has an area of less than 3 km^2. With this small footprint, around 20% to 30% of these soundings are sufficiently cloud free to yield full column estimates of XCO_2. To detect CO_2 variations over dark, ocean, or ice-covered surfaces, OCO-2 can point the instrument's field of view toward the bright ocean glint spot over almost 90% of the range of latitudes on the sunlit hemisphere. With these capabilities, OCO-2 provides substantially better coverage than previous missions, providing snapshots of most robust features of the carbon cycle (Crowell et al., 2019; Peiro et al., 2022), as well as new insights into the response of the carbon cycle to natural and anthropogenic perturbations (Chatterjee et al., 2017; Liu et al., 2017; Weir et al., 2021). GOSAT and OCO-2 have recently been joined by their sister missions, GOSAT-2 (2018) and OCO-3 (2019), on the International Space Station, providing additional coverage and resolution. For example, OCO-3 includes a new observation mode, called the Snapshot Area Map (SAM) mode, dedicated to mapping out larger spatial-scale emitters like cities and power plants. The SAM mode can be used to map areas of up to 100 × 100 km^2 on the Earth's surface with the standard OCO-3 ground footprints of 2 × 2 km^2, providing unprecedented high spatial resolution coverage of large-scale CO_2 emitters worldwide (Eldering et al., 2019; Kiel et al., 2021; Nassar et al., 2022).

GOSAT, GOSAT-2, OCO-2, and OCO-3 are pioneering missions that have demonstrated the capability of a space-based remote sensing greenhouse gas monitoring network. Relative to the ground-based monitoring stations, satellites provide dense global coverage in both space and time, although the most useful observations for retrieving CO_2 concentrations are limited to areas under clear-sky conditions. However, satellite retrievals have higher uncertainty associated with the retrievals (ranging from 0.25% for current OCO-2/3 retrievals to 0.5% for current GOSAT retrievals), as well as systematic biases due to interference from aerosols, cloud, and surface conditions, among other factors. This trade-off between coverage and accuracy/precision can best be reconciled by using information from both satellite retrievals and the ground-based monitoring network for deriving regional to global surface flux estimates (Byrne et al., 2022; Phillip et al., 2022).

Ground-Based Remote Sensing Observations of Atmospheric CO_2

The ground-based remote sensing greenhouse gas monitoring networks record direct solar absorption spectra from which column-averaged dry-air mole fractions of CO_2 are retrieved using various algorithms. The ground-based column measurements help to disentangle the effects of atmospheric mixing from surface exchanges and complement the in situ measurements made from surface or airborne platforms (figure 1). Due to the vertical integration of the CO_2 concentrations above the surface covering the whole atmosphere, these measurements are much less affected by vertical transport than surface in situ measurements. The measured horizontal gradients are more directly related to the underlying regional-scale fluxes of CO_2 (Yang et al.,

2007). As the latitudinal gradient and temporal variations in XCO_2 are small, these measurements require high precision and accuracy. Satellites provide global XCO_2 measurements at high spatial resolution, but the retrieval is dependent on several parameters (e.g., surface conditions, atmospheric conditions, and spectroscopy). The accuracy requirements for satellite data are very demanding as small errors in the retrieved XCO_2 may result in significant errors in the derived fluxes (Chevallier et al., 2007). The XCO_2 measurements from ground-based remote sensing networks are ideal reference measurements for the satellite data to detect and quantify any temporal drifts and spatial biases and their dependency on the retrieval parameters.

The Total Carbon Column Observing Network (TCCON), a ground-based remote sensing greenhouse gas monitoring network, was founded in 2004 to support satellite validation and carbon cycle research. Figure 8 shows the TCCON XCO_2 data coverage as a function of latitude since the start of the network. Currently, about 28 stations are operational globally. TCCON provides long and quasi-continuous time series of precise and accurate concentrations of XCO_2, among other gases, by performing profile scaling retrieval of measured spectra in the near-infrared (NIR) using high-resolution (0.02 cm^{-1}) Fourier transform infrared (FTIR) spectrometers (Wunch et al., 2011). TCCON provides XCO_2 by taking the ratio of CO_2 retrieved from the 6,300 cm^{-1} band to the simultaneously measured O_2 from the 7,885 cm^{-1} band. The XCO_2 values are then calibrated to the World Meteorological Organization (WMO) standard reference scale using an empirical scaling factor calculated from vertically resolved in situ measurements performed from airborne platforms at several sites. The scaling factor, 0.9898 ± 0.001, is uniform for all sites (Wunch et al., 2015). The total uncertainty budget for the present version (GGG2014) of XCO_2 data is about 0.2%. Further efforts are made to decrease any station-to-station biases by carefully monitoring the instrumental line shape with reference cell measurements (Hase et al., 2013), nonlinearity checks, and side-by-side measurements using portable FTIR spectrometers as the traveling standard instrument developed as part of the ESA's Fiducial Reference Measurements for Greenhouse Gases (FRM4GHG) project (Sha et al., 2020).

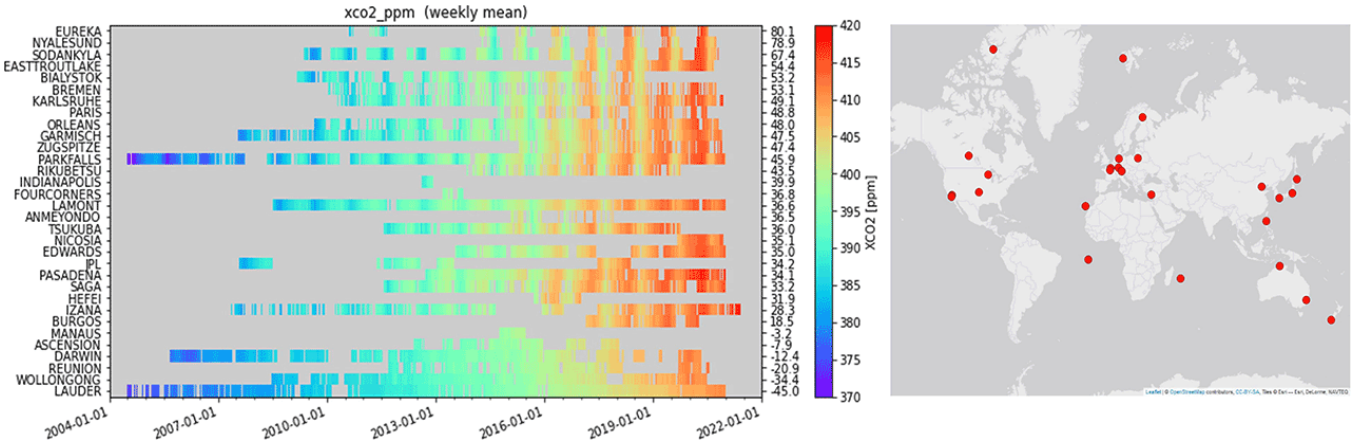

Figure 8. TCCON XCO_2 data coverage as a function of latitude, with site locations shown on the map.

Source: Image generated by authors.

The Collaborative Carbon Column Observing Network (COCCON) is an emerging network complementary to TCCON, providing measurements of XCO_2, among other gases, by performing profile scaling retrieval of measured spectra in the NIR using portable lightweight, low-resolution (0.5 cm^{-1}) FTIR spectrometers (Frey et al., 2019). The low-resolution instruments have shown performances for the retrieved XCO_2 product similar to the high-resolution TCCON (Sha et al., 2020). The measurements are linked to the WMO scale via calibration of the COCCON spectrometers to the TCCON and making use of the TCCON versus in situ calibration (Alberti et al., 2022). Currently, more than 60 spectrometers are operating around the globe forming the COCCON <http://www.imk-asf.kit.edu/english/COCCON.php> collaborative network (Alberti et al., 2022; Frey et al., 2015). The portable spectrometers are used to quantify localized sources of greenhouse gases using an array of several spectrometers (Hase et al., 2015), operated on onboard moving platforms like cars (Butz et al., 2017) or ships (Knapp et al., 2021) or as permanent stations in remote locations (Frey et al., 2021). The instrumental line shape monitoring is performed using open path measurements and recently also with a C_2H_2 cell (Alberti et al., 2022; Frey et al., 2015).

The Infrared Working Group of the Network for the Detection of Atmospheric Composition Change (NDACC) is a network of high-resolution FTIR spectrometers that records direct solar absorption spectra in the mid-infrared (MIR) spectral range (De Mazière et al., 2018). Barthlott et al. (2015) developed a strategy to retrieve XCO_2 by performing profile scaling retrievals of the measured spectra in a spectral region around 2,600–3,000 cm^{-1}. Buschmann et al. (2016) reported that the NDACC XCO_2 showed scatter of about 3‰ compared to a model output using data from 10 stations since 1996. The comparison to collocated TCCON XCO_2 showed a scatter of 4‰ for daily and monthly means, indicating stability of the difference and a bias of 25‰, which is most likely due to errors in MIR spectroscopy of CO_2 parameters. The NDACC XCO_2 averaging kernels (indicating the retrieval sensitivity) showed a higher sensitivity at lower atmospheric pressure in the stratosphere and a lower sensitivity in the troposphere (by a factor of 2) as compared to TCCON (Buschmann et al., 2016). The XCO_2 retrieval strategy tested on MIR solar absorption measurements aims toward extending the method to FTIR measurements made since the late 1950s, thereby creating a long-time series record. The NDACC stations add to currently more than 20 FTIR spectrometers providing long-term data.

The ground-based FTIR networks provide long-term data of XCO_2 for detecting changes and trends in the integrated column of the atmosphere with high precision and intercalibration accuracy. The networks follow strict measurement and data protocols to ensure high data quality and consistency across the network. They provide important reference data to validate atmospheric CO_2 measurements from satellites, fill gaps in satellite observations, produce validation and development support for models, improve the understanding of the carbon cycle, and provide a transfer standard between the satellite measurements and ground-based in situ networks. The recent developments of more compact, portable, and less expensive FTIR spectrometers will enhance their deployment in developing countries to remote areas on a campaign or long-term deployment basis.

Interannual Variability and Long-Term Trend of Atmospheric CO_2

From the combination of CO_2 measurements deduced from ice cores and atmospheric measurements initiated at the end of the 1960s, it is known that the CO_2 content has increased by 47% since 1850 (figure 9A), going from an average concentration of around 280 ppm in 1850 (Rubino et al., 2019) to 413 ppm in 2020 (WMO, 2021). According to the observations, the rate of CO_2 increases in the atmosphere remained below 1 ppm/year until the end of the 1960s. The increase in CO_2 then accelerated to reach a rate of 2.2 ppm/year during the past decade (figure 9C). It is essential to understand that given the CO_2 emissions by human activities (figure 9B), it would make sense to have a CO_2 growth rate in the atmosphere twice as high than what is measured. Only around 45% of the CO_2 emitted by human activities remain in the atmosphere, while the rest is absorbed by the oceans and the land biota (Friedlingstein et al., 2022). The airborne fraction is defined as the ratio between the atmospheric growth rate and the anthropogenic emissions (Knorr, 2009), and any change in this ratio should be closely monitored as it provides a diagnostic of the intensity of carbon sinks at the global scale (van Marle et al., 2022).

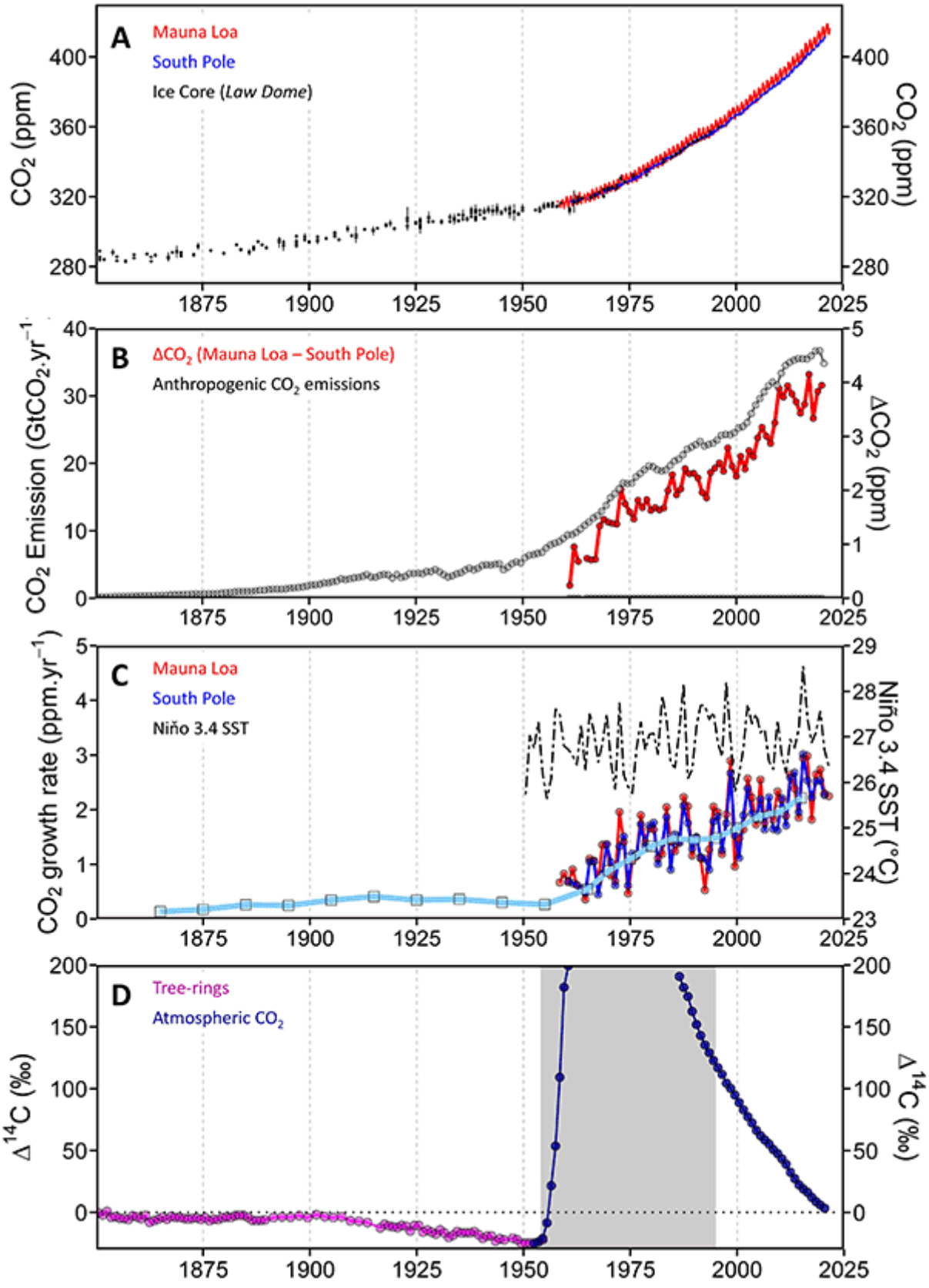

Figure 9. (A) Atmospheric CO_2 mole fractions since 1850 from the Law Dome ice core in Antarctica (Rubino et al., 2019) and from in situ measurements at Mauna Loa and South Pole (Keeling et al., 2001). (B) Annual emissions of fossil fuel CO_2 (Andrew & Peters, 2021) in gray and atmospheric CO_2 gradient between Mauna Loa and South Pole in red. (C) CO_2 growth rate calculated from Mauna Loa (red) and South Pole observations (blue). The light blue curve is

the growth rate calculated from the combination of ice core and South Pole data set averaged per decade. The black curve shows the Niño 3.4 index. (D) $^{14}C/C$ ratio in annual tree rings (Stuiver & Quay, 1981) and since 1954 in atmospheric CO_2 (Graven et al., 2017; Levin et al., 2022).

Source: Image generated by authors.

Averaged over 5-year periods, the CO_2 growth rate has been increasing quite regularly since the early 1960s, with a noticeable slowdown between 1985 and 1995. This episode is attributed to the eruption of Mount Pinatubo in June 1991, which injected aerosols into the stratosphere, causing large-scale cooling on the order of -0.5°C (Dutton & Christy, 1992). This cooling, together with the modification of the incident solar flux, has stimulated the net uptake of carbon by the oceans and terrestrial ecosystems—in particular, a reduction in soil respiration (Angert et al., 2004; Lucht et al., 2002). Continuous measurements also make it possible to highlight interannual variability in CO_2 growth rates, on average ± 0.4 ppm around average values. As can be seen with the example of the Mauna Loa and South Pole stations (figure 9C), this variability appears very consistent from one station to another, clearly indicating a large-scale process at the origin of this variability. Furthermore, this variability observed in the atmosphere cannot be explained by the CO_2 emissions linked to the use of fossil fuels, which shows a low interannual variability (figure 9B). Actually, the highest year-to-year change in anthropogenic emissions occurred in 2020, with a 5% to 8% decrease, as a result of the lockdowns established in most countries to reduce the spread of the COVID-19 virus (Le Quéré et al., 2020; Liu et al., 2020). However, due to the very large reservoir, this drastic reduction has hardly any effect on the atmospheric CO_2 burden, as it is masked by the larger natural interannual variability (Vermeulen et al., 2020). This variability must therefore be explained by the so-called natural carbon reservoirs (oceans and terrestrial ecosystems) and the atmosphere–ocean/ecosystem exchanges to explain this variability. An important point to note is the correlation between periods of strong CO_2 growth in the atmosphere (figure 9C) and El Niño–Southern Oscillation, characterized by a significant anomaly in the equatorial and tropical climate system (figure 9C). Relatively high CO_2 growth rates have been detected by surface networks and, more recently, by the satellite observations, for example, during the El-Niño years in 1982/1983 (Gaudry et al., 1987), 1986/1987 (Wong et al., 1993), 1997/1998 (Gurney et al., 2008), and 2015/2016 (Betts et al., 2016; Chatterjee et al., 2017). Many studies have therefore sought to understand the relationship between El-Niño climate anomalies and the carbon cycle (Bacastow, 1976; Bousquet et al., 2000; Gurney et al., 2008; Jones & Friedlingstein, 2020; Keeling & Revelle, 1985; Kim et al., 2016; Rödenbeck et al., 2018). Each El-Niño episode has its own characteristics in terms of intensity and localization, but overall, the increase in CO_2 growth rates following an El-Niño is partly explained by an increase in the oceanic CO_2 degassing flux and, above all, by a disturbance of the terrestrial biospheric fluxes. Temperature and precipitation anomalies typical of El-Niño cause an increase in net fluxes of CO_2 to the atmosphere through various processes, including reduced photosynthesis, increased soil respiration, and fires. The study of the interannual variability of CO_2 is important because it provides large-scale experiments of the link between climate and CO_2, experiments allowing the validation of biogeochemical models of the carbon cycle.

Coming back to the long-term increase in atmospheric CO_2, a slightly stronger trend in the stations of the Northern Hemisphere is observed, which translates into an increase in the hemispheric gradient observed, for example, between Mauna Loa and the South Pole, on average, by 0.53 ppm per decade (figure 9B). This signal is closely correlated with the increase in anthropogenic CO_2 emissions, which are largely located in the Northern Hemisphere, by 0.45 ± 0.01 $ppm \cdot PgC^{-1} \cdot year^{-1}$ (Ciais et al., 2019; Conway & Tans, 1999; Keeling & Graven, 2021). However, the increase of the latitudinal CO_2 gradient in the atmosphere is lower than it should be, given the increase in anthropogenic CO_2 emissions alone. The differential must be explained either by a reduction in the oceanic carbon sink, which is not what oceanographic observations indicate (Landschützer et al., 2015; Le Quéré et al., 2007; Watson et al., 2020), or by an increase in carbon sinks in the Northern Hemisphere. A detailed study of CO_2 gradients highlights the increase in the terrestrial carbon sink to explain the observed atmospheric signals, involving processes such as a fertilization effect linked to the increase in CO_2 contents and nitrogen deposition, a climate change effect, and an effect of reforestation (Ciais et al., 2019). Another atmospheric signal, not detailed here, also points to an increase in carbon fluxes exchanged with the terrestrial ecosystems of the Northern Hemisphere, as indicated by an increase of up to 50% in the seasonal amplitude of CO_2 since 1960, at high northern latitudes (Graven et al., 2013; Keeling et al., 1996).

$^{14}CO_2$ Observations

Radiocarbon (^{14}C) is the long-lived radioactive isotope of carbon that is naturally produced in the upper atmosphere by reaction of cosmogenically produced neutrons with atmospheric nitrogen (Kovaltsov et al., 2012; Lingenfelter, 1963). After its oxidation to CO_2, $^{14}CO_2$ participates in all CO_2 exchange processes similar to the stable CO_2 molecules. The radioactive half-life time of ^{14}C is 5,700 ± 30 years. The natural abundance of ^{14}C in modern carbon and atmospheric CO_2 is only about $^{14}C/C \approx 10^{-12}$, corresponding to the equilibrium between production in the atmosphere and its radioactive decay in all carbon reservoirs that exchange CO_2 with this reservoir.

Shortly after publication of the first analyses of radiocarbon in natural carbon compartments (Anderson et al., 1951), first precise measurements of atmospheric $^{14}CO_2$ were conducted in 1954 at a coastal site close to Wellington, New Zealand (Rafter & Fergusson, 1957). Further measurements at a number of stations in Northern and Southern Hemisphere air started in 1959 by Münnich and Vogel (1963). Already in the mid-1950s, it was realized that the atmospheric equilibrium $^{14}C/C$ ratio had been perturbed by human activities: (a) As a consequence of the ongoing input of ^{14}C-free CO_2 from fossil fuel burning into the atmosphere, not only the CO_2 concentration had increased (see above), but its $^{14}C/C$ ratio also had decreased significantly; this decrease is known as Suess effect (Suess, 1955). (b) Through artificial production of ^{14}C during the atmospheric nuclear weapon tests (Libby, 1956) in the 1950s and 1960s, the $^{14}C/C$ ratio in tropospheric CO_2 increased rapidly to about a factor of 2 in the Northern Hemisphere. Figure 9D shows the development of $\Delta^{14}C$ in atmospheric CO_2 since 1860. $\Delta^{14}C$ is defined as the relative deviation of the $^{14}C/C$ ratio of a sample from a reference material in permil (‰; see Stuiver & Polach, 2016). The reference material has the approximate $^{14}C/C$ ratio of atmospheric CO_2 before

perturbation; it defines the zero point of the Δ scale. $\Delta^{14}C$ data before 1954 have been derived from analyses on tree rings (Stuiver & Quay, 1981). The significant decrease of the $^{14}C/C$ ratio is best visible since about 1900 coincides with the increase of anthropogenic CO_2 emissions and the rise of atmospheric CO_2. The Suess effect is one of the most convincing arguments that the global rise of CO_2 since industrialization is indeed humanmade and due to fossil fuel CO_2 emissions, because only ^{14}C-free CO_2 can cause a decrease of the $^{14}C/C$ ratio.

After 1955, a steep global $\Delta^{14}C$ increase by more than 100‰ within a few years only is observed. This increase continued in the Northern Hemisphere troposphere up to 1,000‰ in 1963 (a factor of 2 of the $^{14}C/C$ ratios compared to the natural equilibrium value). Figure 10 shows this development of the so-called bomb $^{14}CO_2$ spike in the troposphere of both hemispheres. While the Northern Hemisphere bomb perturbation reached its maximum in 1963, the $\Delta^{14}C$ values in the Southern Hemisphere increased only with a delay of about 1–2 years, with the maximum reaching only values up to 700‰. This delay and smaller maximum are because most of the bomb tests were conducted in the Northern Hemisphere, and the $^{14}CO_2$ bomb perturbation, now diluted, reached the Southern Hemisphere only through interhemispheric air mass exchange or by horizontal and downward mixing of stratospheric air into the (Southern Hemisphere) troposphere. Note that most of the bomb ^{14}C was injected into the Northern Hemisphere stratosphere by the most powerful nuclear tests. The seasonal downward movement of ^{14}C-enriched stratospheric air into the troposphere manifested itself in the $\Delta^{14}C$ increases during spring in the first years after the nuclear test ban treaty in 1963 (Telegadas, 1971). This dynamical behavior of bomb $^{14}CO_2$ in the global atmosphere was used to calibrate or validate atmospheric transport parameters in global models (e.g., Johnston, 1989; Kjellström et al., 2000; Levin et al., 2010).

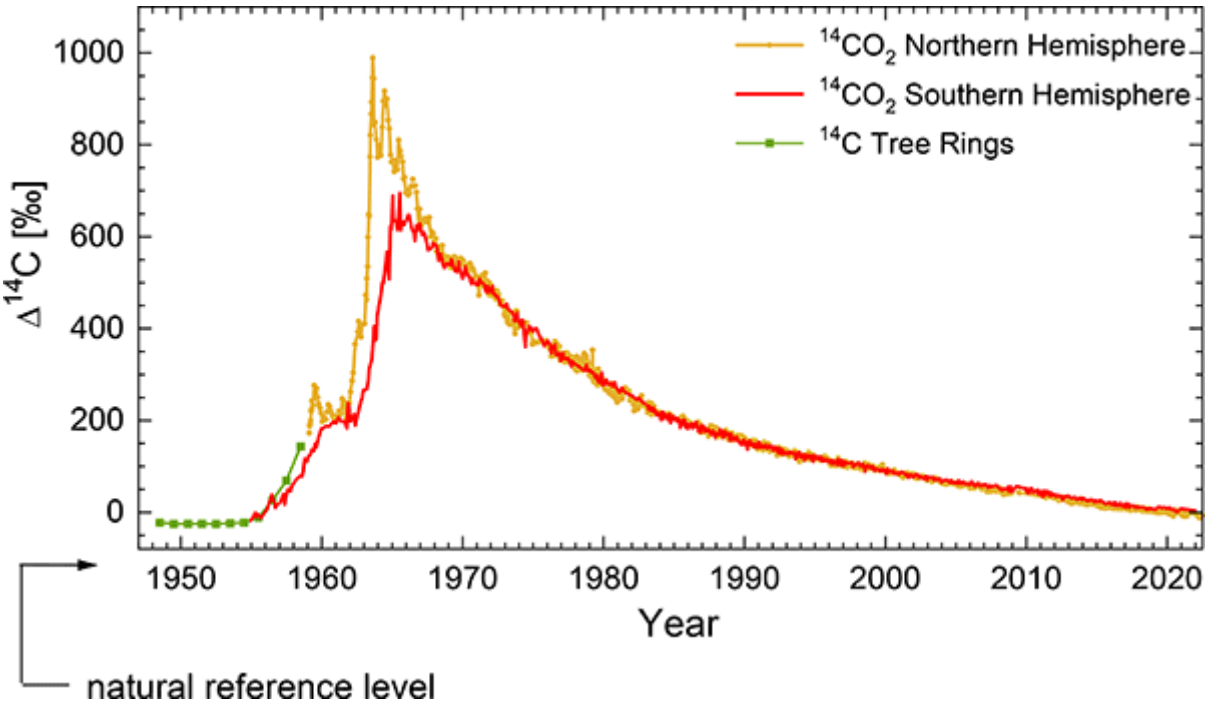

Figure 10. Tropospheric $\Delta^{14}C\text{-}CO_2$ in the Northern and Southern Hemispheres since the start of the atmospheric nuclear bomb tests. The natural reference level (0‰) corresponds to the approximate equilibrium between ^{14}C production in the atmosphere and ^{14}C decay in all carbon reservoirs. Tree ring data are from Stuiver and Quay (1981), Southern Hemisphere data until 1983 from Turnbull et al. (2017), Northern Hemisphere data until 1983 from Levin et al. (1985), and all other data from Levin et al. (2022).

Source: Image generated by authors.

After the ban on aboveground nuclear bomb tests (1963), from about 1965, $\Delta^{14}CO_2$ decreased in both hemispheres due to large gross CO_2 exchange fluxes between atmosphere, biosphere, and oceans. Further, since about 1970, the $^{14}CO_2$ perturbation has been almost evenly distributed in the troposphere between both hemispheres. Only very tiny differences of a few ‰ are still observed between the Northern Hemisphere, the tropics, and the Southern Hemisphere (Levin et al., 2022). The ongoing decrease of $\Delta^{14}CO_2$ even after 1995, when atmosphere, biosphere, and oceans have largely equilibrated, is again due to the ongoing and further increasing input of ^{14}C-free fossil CO_2 into the atmosphere (Graven, 2015; Levin et al., 2010).

Perspectives

The hope of the scientific community in the 2000s, when new continental sites were being installed, was to quickly reduce the uncertainty with which Northern Hemisphere regions and ecosystems were emitting more CO_2, at a scale of a few thousand kilometers. This hope has not materialized, mainly because models showed large errors in simulating long-range and vertical atmospheric transport, and such errors have not reduced much over the past 20 years and to a smaller extent, because some regions like northern Eurasia remained undersampled. The relative failure of regional CO_2 inversions has not slowed down attempts to constrain CO_2 fluxes at a finer regional scale, a few hundred kilometers, using mesoscale atmospheric networks. Over flat terrain, CO_2 is quickly depleted as an air mass moves over a sink area, typically by about 1 ppm over 100 km. Mesoscale models were used to exploit CO_2 gradients of that type measured by aircraft over the United States during the COBRA campaign (Gerbig et al., 2003) and over southwestern France during the CERES campaign (Dolman et al., 2006; Lauvaux et al., 2008). To move from costly and sporadic aircraft campaigns to continuous measurements, dense regional "mesoscale" networks at tall towers were deployed in the U.S. Great Plains (Lauvaux et al., 2012; Miles et al., 2012) and in western Europe as part of ICOS (Heiskanen et al., 2022; Ramonet et al., 2020). In this new step toward the regionalization of carbon fluxes, there is no doubt that satellites will also have an important role to play, even if to date, the detection of regional CO_2 flux anomalies remains a real challenge (Buchwitz et al., 2021; Philip et al., 2022). Major projects are under way to establish an integrated approach, using both in situ surface and airborne measurements, remote sensing ground-based and satellite observations, and statistical inventories and atmospheric circulation models, to develop verification of anthropogenic emissions of CO_2 and their reduction in response to measures taken by the countries. A constellation of satellites dedicated to CO_2 imagery (CO2M) is programmed by the European Commission, within the framework of the Copernicus program, to provide estimates of CO_2 emissions from 2026 onward (Janssens-Maenhout et al., 2020). On an even finer spatial scale,

several research projects have been implemented for the coming few years to develop measurements of atmospheric CO_2 in urban areas, to improve the monitoring of urban emissions, in association with statistical emission inventories. A pioneering program in this field has been deployed around Indianapolis (INFLUX program), combining surface, airborne, and radiocarbon measurements, demonstrating an optimal detection potential of few percent of CO_2 emission trends (Lauvaux et al., 2020; Turnbull et al., 2019). There remain, however, many challenges—in particular, to better differentiate biospheric fluxes from anthropogenic emissions—a challenge that several research groups are now tackling around cities such as Los Angeles (Miller et al., 2020), Boston (Sargent et al., 2018), Paris (Lian et al., 2022), London (Pitt et al., 2019), Mexico City (González del Castillo et al., 2021), Beijing (Zheng et al., 2020), and Seoul (Park et al., 2021).

Further Reading

Canadell, J. G., Monteiro, P. M. S., Costa, M. H., Cotrim da Cunha, L., Cox, P. M., Eliseev, A. V., Henson, S., Ishii, M., Jaccard, S., Koven, C., Lohila, A., Patra, P. K., Piao, S., Rogelj, J., Syampungani, S., Zaehle, S., & Zickfeld, K. (2021, August 9). *Global carbon and other biogeochemical cycles and feedbacks*. Climate Change 2021: The Physical Science Basis. Contribution of Working Group I to the Sixth Assessment Report of the Intergovernmental Panel on Climate Change (V. Masson-Delmotte, P. Zhai, A. Pirani, S. L. Connors, C. Péan, S. Berger, N. Caud, Y. Chen, L. Goldfarb, M. I. Gomis, M. Huang, K. Leitzell, E. Lonnoy, J. B. R. Matthews, T. K. Maycock, T. Waterfield, O. Yelekçi, R. Yu, & B. Zhou, Eds.). Cambridge University Press.

Friedlingstein, P., Jones, M. W., O'Sullivan, M., Andrew, R. M., Bakker, D. C. E., Hauck, J., Le Quéré, C., Peters, G. P., Peters, W., Pongratz, J., Sitch, S., Canadell, J. G., Ciais, P., Jackson, R. B., Alin, S. R., Anthoni, P., Bates, N. R., Becker, M., Bellouin, N., . . . Zeng, J.. Global carbon budget: 2021 <https://doi.org/10.5194/essd-14-1917-2022,%202022>. *Earth System Science Data*, *14*, 1917–2005.

Masson-Delmotte, V., Zhai, P., Pirani, A., Connors, S. L., Péan, C., Berger, S., Caud, N., Chen, Y., Goldfarb, L., Gomis, M. I., Huang, M., Leitzell, K., Lonnoy, E., Matthews, J. B. R., Maycock, T. K., Waterfield, T., Yelekçi, O., Yu, R., & Zhou, B. (Eds.). (2021, August 9). *Climate change 2021—The physical science basis*. Contribution of Working Group I to the Sixth Assessment Report of the Intergovernmental Panel on Climate Change. Cambridge University Press.

Pinty, B., Ciais, P., Dee, D., Dolman, H., Dowell, M., Engelen, R., Holmlund, K., Janssens-Maenhout, G., Meijer, Y., Palmer, P., Scholze, M., Denier van der Gon, H., Heimann, M., Juvyns, O., Kentarchos, A., & Zunker, H. (2019). *An operational anthropogenic CO_2 emissions monitoring & verification support capacity—Needs and high level requirements for in situ measurements* <https://doi.org/10.2760/182790> (EUR 29817 EN). European Commission Joint Research Centre.

References

Ahn, J., Brook, E. J., Mitchell, L., Rosen, J., McConnell, J. R., Taylor, K., Etheridge, D., & Rubino, M. (2012). Atmospheric CO2 over the last 1000 years: A high-resolution record from the West Antarctic Ice Sheet (WAIS) divide ice core <https://doi.org/10.1029/2011GB004247>. *Global Biogeochemical Cycles*, *26*(2).

Alberti, C., Hase, F., Frey, M., Dubravica, D., Blumenstock, T., Dehn, A., Castracane, P., Surawicz, G., Harig, R., Baier, B. C., Bès, C., Bi, J., Boesch, H., Butz, A., Cai, Z., Chen, J., Crowell, S. M., Deutscher, N. M., Ene, D., . . . Orphal, J. (2022).

Improved calibration procedures for the EM27/SUN spectrometers of the COllaborative Carbon Column Observing Network (COCCON) <https://doi.org/10.5194/amt-15-2433-2022>. *Atmospheric Measurement Techniques*, *15*(8), 2433–2463.

Anderson, B. E., Collins, J. E., Sachse, G. W., Whiting, G. W., Blake, D. R., & Rowland, F. S. (1993). AASE-II observations of trace carbon species distributions in the mid to upper troposphere <https://doi.org/10.1029/93GL01693>. *Geophysical Research Letters*, *20*(22), 2539–2542.

Anderson, E. C., Arnold, J. R., & Libby, W. F. (1951). Measurement of low level radiocarbon <https://doi.org/10.1063/1.1745896>. *Review of Scientific Instruments*, *22*(4), 225–230.

Andrew, R., & Peters, G. (2021). *The Global Carbon Project's fossil CO2 emissions dataset* <https://doi.org/10.6084/m9.figshare.16729084.v1> (figshare, Ed.). CICERO Center for International Climate Research.

Andrews, A. E., Boering, K. A., Daube, B. C., Wofsy, S. C., Loewenstein, M., Jost, H., Podolske, J. R., Webster, C. R., Herman, R. L., Scott, D. C., Flesch, G. J., Moyer, E. J., Elkins, J. W., Dutton, G. S., Hurst, D. F., Moore, F. L., Ray, E. A., Romashkin, P. A., & Strahan, S. E. (2001). Mean ages of stratospheric air derived from in situ observations of CO2, CH4, and N2O <https://doi.org/10.1029/2001JD000465>. *Journal of Geophysical Research: Atmospheres*, *106*(D23), 32295–32314.

Andrews, A. E., Kofler, J. D., Trudeau, M. E., Williams, J. C., Neff, D. H., Masarie, K. A., Chao, D. Y., Kitzis, D. R., Novelli, P. C., Zhao, C. L., Dlugokencky, E. J., Lang, P. M., Crotwell, M. J., Fischer, M. L., Parker, M. J., Lee, J. T., Baumann, D. D., Desai, A. R., Stanier, C. O., . . . Tans, P. P. (2014). CO2, CO, and CH4 measurements from tall towers in the NOAA earth system research laboratory's global greenhouse gas reference network: Instrumentation, uncertainty analysis, and recommendations for future high-accuracy greenhouse gas monitoring efforts. *Atmospheric Measurement Techniques*, *7*(2), 647–687.

Angert, A., Biraud, S., Bonfils, C., Buermann, W., & Fung, I. (2004). CO2 seasonality indicates origins of post-Pinatubo sink <https://doi.org/10.1029/2004GL019760>. *Geophysical Research Letters*, *31*(11).

Bacastow, R. B. (1976). Modulation of atmospheric carbon dioxide by the Southern Oscillation <https://doi.org/10.1038/261116a0>. *Nature*, *261*(5556), 116–118.

Baer, D., Gupta, M., Owano, T., & O'Keefe, A. (2004, February 9). *Cavity-enhanced instrumentation for atmospheric monitoring* [Paper presented]. Laser Applications to Chemical and Environmental Analysis, Annapolis, Maryland, United States.

Baier, B. C., Sweeney, C., & Chen, H. (2023). The AirCore atmospheric sampling system <https://doi.org/10.1029/2019JD031339>. In N. R. Nalli (Ed.), *Field measurements for passive environmental remote sensing* (pp. 139–156). Elsevier.

Baier, B. C., Sweeney, C., Choi, Y., Davis, K. J., DiGangi, J. P., Feng, S., Fried, A., Halliday, H., Higgs, J., Lauvaux, T., Miller, B. R., Montzka, S. A., Newberger, T., Nowak, J. B., Patra, P., Richter, D., Walega, J., & Weibring, P. (2020). Multispecies assessment of factors influencing regional CO2 and CH4 enhancements during the winter 2017 ACT-America campaign. *Journal of Geophysical Research: Atmospheres*, *125*(2), e2019JD031339.

Baker, D. F., Law, R. M., Gurney, K. R., Rayner, P., Peylin, P., Denning, A. S., Bousquet, P., Bruhwiler, L., Chen, Y. H., Ciais, P., Fung, I. Y., Heimann, M., John, J., Maki, T., Maksyutov, S., Masarie, K., Prather, M., Pak, B., Taguchi, S., & Zhu, Z.

(2006). TransCom 3 inversion intercomparison: Impact of transport model errors on the interannual variability of regional CO2 fluxes, 1988–2003 <https://doi.org/10.1029/2004GB002439>. *Global Biogeochemical Cycles*, *20*(1).

Baker, F. W. G. (2009). The first international polar year (1882–1883): French measurements of carbon dioxide concentrations in the atmosphere at Bahia Orange, Hoste Island, Tierra del Fuego <https://doi.org/10.1017/S0032247408008176>. *Polar Record*, *45*(3), 265–268.

Bakwin, P. S., Tans, P. P., Hurst, D. F., & Zhao, C. (1998). Measurements of carbon dioxide on very tall towers: Results of the NOAA/CMDL program. *Tellus*, *50B*, 401–415.

Barthlott, S., Schneider, M., Hase, F., Wiegele, A., Christner, E., González, Y., Blumenstock, T., Dohe, S., García, O. E., Sepúlveda, E., Strong, K., Mendonca, J., Weaver, D., Palm, M., Deutscher, N. M., Warneke, T., Notholt, J., Lejeune, B., Mahieu, E., . . . Raffalski, U. (2015). Using XCO2 retrievals for assessing the long-term consistency of NDACC/FTIR data sets <https://doi.org/10.5194/amt-8-1555-2015>. *Atmospheric Measurement Techniques*, *8*(3), 1555–1573.

Basu, S., Guerlet, S., Butz, A., Houweling, S., Hasekamp, O., Aben, I., Krummel, P., Steele, P., Langenfelds, R., Torn, M., Biraud, S., Stephens, B., Andrews, A., & Worthy, D. (2013). Global CO2 fluxes estimated from GOSAT retrievals of total column CO2 <https://doi.org/10.5194/acp-13-8695-2013>. *Atmospheric Chemistry and Physics*, *13*(17), 8695–8717.

Belikov, D., Arshinov, M., Belan, B., Davydov, D., Fofonov, A., Sasakawa, M., & Machida, T. (2019). Analysis of the diurnal, weekly, and seasonal cycles and annual trends in atmospheric CO2 and CH4 at tower network in Siberia from 2005 to 2016. *Atmosphere*, *10*(11), 689.

Berner, W., Oeschger, H., & Stauffer, B. (1980). Information on the CO2 cycle from Ice Core studies <https://doi.org/10.1017/S0033822200009498>. *Radiocarbon*, *22*(2), 227–235.

Betts, R. A., Jones, C. D., Knight, J. R., Keeling, R. F., & Kennedy, J. J. (2016). El Niño and a record CO2 rise <https://doi.org/10.1038/nclimate3063>. *Nature Climate Change*, *6*(9), 806–810.

Bischof, W. (1962). Variations in concentration of carbon dioxide in the free atmosphere <https://doi.org/10.3402/tellusa.v14i1.9529>. *Tellus*, *14*(1), 87–90.

Bischof, W. (1970). Carbon dioxide measurements from aircraft <https://doi.org/10.3402/tellusa.v22i5.10249>. *Tellus*, *22*(5), 545–549.

Bischof, W., & Bolin, B. (1966). Space and time variations of the CO2 content of the troposphere and lower stratosphere <https://doi.org/10.1111/j.2153-3490.1966.tb00221.x>. *Tellus*, *18*(2–3), 155–159.

Boering, K. A., Daube, B. C., Jr., Wofsy, S. C., Loewenstein, M., Podolske, J. R., & Keim, E. R. (1994). Tracer-tracer relationships and lower stratospheric dynamics: CO2 and N2O correlations during SPADE <https://doi.org/10.1029/94GL01985>. *Geophysical Research Letters*, *21*(23), 2567–2570.

Bolin, B., & Bischof, W. (1970). Variations of the carbon dioxide content of the atmosphere in the northern hemisphere <https://doi.org/10.1111/j.2153-3490.1970.tb00508.x>. *Tellus*, *22*(4), 431–442.

Bousquet, P., Peylin, P., Ciais, P., Le Quéré, C., Friedlingstein, P., & Tans, P. P. (2000). Regional changes in carbon dioxide fluxes of land and oceans since 1980. *Science*, *290*, 1342–1346.

Bovensmann, H., Burrows, J. P., Buchwitz, M., Frerick, J., Noël, S., Rozanov, V. V., Chance, K. V., & Goede, A. P. H. (1999). SCIAMACHY: Mission objectives and measurement modes <https://doi.org/10.1175/1520-0469(1999)056%3c0127:SMOAMM%3e2.0.CO;2>. *Journal of the Atmospheric Sciences*, *56*(2), 127–150.

Broquet, G., Chevallier, F., Bréon, F.-M., Kadygrov, N., Alemanno, M., Apadula, F., Hammer, S., Haszpra, L., Meinhardt, F., Morguí, J., Necki, J., Piacentino, S., Ramonet, M., Schmidt, M., Thompson, R., Vermeulen, A., Yver, C., & Ciais, P. (2013). Regional inversion of CO2 ecosystem fluxes from atmospheric measurements: Reliability of the uncertainty estimates <https://doi.org/10.5194/acp-13-9039-2013>. *Atmospheric Chemistry and Physics*, *13*(17), 9039–9056.

Buchwitz, M., Reuter, M., Noël, S., Bramstedt, K., Schneising, O., Hilker, M., Fuentes Andrade, B., Bovensmann, H., Burrows, J. P., Di Noia, A., Boesch, H., Wu, L., Landgraf, J., Aben, I., Retscher, C., O'Dell, C. W., & Crisp, D. (2021). Can a regional-scale reduction of atmospheric CO2 during the COVID-19 pandemic be detected from space? A case study for East China using satellite XCO2 retrievals <https://doi.org/10.5194/amt-14-2141-2021>. *Atmospheric Measurement Techniques*, *14*(3), 2141–2166.

Buschmann, M., Deutscher, N. M., Sherlock, V., Palm, M., Warneke, T., & Notholt, J. (2016). Retrieval of xCO2 from ground-based mid-infrared (NDACC) solar absorption spectra and comparison to TCCON <https://doi.org/10.5194/amt-9-577-2016>. *Atmospheric Measurement Techniques*, *9*(2), 577–585.

Butchart, N. (2014). The Brewer-Dobson circulation <https://doi.org/10.1002/2013RG000448>. *Reviews of Geophysics*, *52*(2), 157–184.

Butz, A., Dinger, A. S., Bobrowski, N., Kostinek, J., Fieber, L., Fischerkeller, C., Giuffrida, G. B., Hase, F., Klappenbach, F., Kuhn, J., Lübcke, P., Tirpitz, L., & Tu, Q. (2017). Remote sensing of volcanic CO2, HF, HCl, SO2, and BrO in the downwind plume of Mt. Etna <https://doi.org/10.5194/amt-10-1-2017>. *Atmospheric Measurement Techniques*, *10*(1), 1–14.

Byrne, B., Baker, D. F., Basu, S., Bertolacci, M., Bowman, K. W., Carroll, D., Chatterjee, A., Chevallier, F., Ciais, P., Cressie, N., Crisp, D., Crowell, S., Deng, F., Deng, Z., Deutscher, N. M., Dubey, M., Feng, S., García, O., Griffith, D. W. T., . . . Zeng, N. (2022). National CO2 budgets (2015–2020) inferred from atmospheric CO2 observations in support of the global stocktake <https://doi.org/10.5194/essd-2022-213>. *Earth System Science Data*.

Callendar, G. S. (1958). On the amount of carbon dioxide in the atmosphere. *Tellus*, *10*(2), 243–248.

Chambers, S. D., Williams, A. G., Conen, F., Griffiths, A. D., Reimann, S., Steinbacher, M., Krummel, P. B., Steele, L. P., van der Schoot, M. V., Galbally, I. E., Molloy, S. B., & Barnes, J. E. (2016). Towards a universal "baseline" characterisation of air masses for high- and low-altitude observing stations using Radon-222 <https://doi.org/10.4209/aaqr.2015.06.0391>. *Aerosol and Air Quality Research*, *16*(3), 885–899.

Chatterjee, A., Gierach, M. M., Sutton, A. J., Feely, R. A., Crisp, D., Eldering, A., Gunson, M. R., O'Dell, C. W., Stephens, B. B., & Schimel, D. S. (2017). Influence of El Niño on atmospheric CO2 over the tropical Pacific Ocean: Findings from NASA's OCO-2 mission <https://doi.org/10.1126/science.aam5776>. *Science*, *358*(6360).

Chen, H., Winderlich, J., Gerbig, C., Hoefer, A., Rella, C. W., Crosson, E. R., Van Pelt, A. D., Steinbach, J., Kolle, O., Beck, V., Daube, B. C., Gottlieb, E. W., Chow, V. Y., Santoni, G. W., & Wofsy, S. C. (2010). High-accuracy continuous airborne measurements of greenhouse gases (CO2 and CH4) using the cavity ring-down spectroscopy (CRDS) technique. *Atmospheric Measurement Techniques*, *3*(2), 375–386.

Chevallier, F., Bréon, F.-M., & Rayner, P. J. (2007). Contribution of the orbiting carbon observatory to the estimation of CO2 sources and sinks: Theoretical study in a variational data assimilation framework <https://doi.org/10.1029/2006JD007375>. *Journal of Geophysical Research: Atmospheres*, *112*(D09307).

Chevallier, F., Engelen, R. J., Carouge, C., Conway, T. J., Peylin, P., Pickett-Heaps, C., Ramonet, M., Rayner, P., & Xueref-Remy, I. (2009). AIRS-based versus flask-based estimation of carbon surface fluxes <https://doi.org/10.1029/2009jd012311>. *Journal of Geophysical Research: Atmospheres*, *114*(D20), D20303.

Ciais, P., Tan, J., Wang, X., Roedenbeck, C., Chevallier, F., Piao, S. L., Moriarty, R., Broquet, G., Le Quéré, C., Canadell, J. G., Peng, S., Poulter, B., Liu, Z., & Tans, P. (2019). Five decades of northern land carbon uptake revealed by the interhemispheric CO2 gradient <https://doi.org/10.1038/s41586-019-1078-6>. *Nature*, *568*(7751), 221–225.

Ciais, P., Tans, P. P., Trolier, M., White, J. W., & Francey, R. (1995). A large Northern Hemisphere terrestrial CO_2 sink indicated by the $^{13}C/^{12}C$ ratio of atmospheric CO_2. *Science*, *269*, 1098–1102.

Conway, T. J., & Tans, P. P. (1999). Development of the CO2 latitude gradient in recent decades <https://doi.org/10.1029/1999GB900045>. *Global Biogeochemical Cycles*, *13*(4), 821–826.

Cox, A., Di Sarra, A. G., Vermeulen, A., Manning, A., Beyersdorf, A., Zahn, A., Manning, A., Watson, A., Karion, A., Hensen, A., Arlyn A., Frumau, A., Colomb, A., Scheeren, B., Law, B., Baier, B., Munger, B., Paplawsky, B., Viner, B., … Loh, Z. (2021). Multi-laboratory compilation of atmospheric carbon dioxide data for the period 1957-2020 <https://doi.org/10.25925/20210801>; obspack_co2_1_GLOBALVIEWplus_v7.0_2021-08-18 [Data set]. NOAA Global Monitoring Laboratory.

Crisp, D., Atlas, R. M., Breon, F. M., Brown, L. R., Burrows, J. P., Ciais, P., Connor, B. J., Doney, S. C. Fung, I. Y., Jacob, D. J., Miller, C. E., O'Brien, D., Pawson, S., Randerson, J. T., Rayner, P., Salawitch, R. J., Sander, S. P., Sen, B., Stephens, G. L., . . . Schroll, S. (2004). The orbiting carbon observatory (OCO) mission <https://doi.org/10.1016/j.asr.2003.08.062>. *Advances in Space Research*, *34*(4), 700–709.

Crosson, E. R. (2008). A cavity ring-down analyzer for measuring atmospheric levels of methane, carbon dioxide, and water vapor <https://doi.org/10.1007/s00340-008-3135-y>. *Applied Physics B-Lasers and Optics*, *92*(3), 403–408.

Crowell, S., Baker, D., Schuh, A., Basu, S., Jacobson, A. R., Chevallier, F., Liu, J., Deng, F., Feng, L., McKain, K., Chatterjee, A., Miller, J. B., Stephens, B. B., Eldering, A., Crisp, D., Schimel, D., Nassar, R., O'Dell, C. W., Oda, T., . . . Jones, D. B. A. (2019). The 2015–2016 carbon cycle as seen from OCO-2 and the global in situ network <https://doi.org/10.5194/acp-19-9797-2019>. *Atmospheric Chemistry and Physics*, *19*(15), 9797–9831.

De Mazière, M., Thompson, A. M., Kurylo, M. J., Wild, J. D., Bernhard, G., Blumenstock, T., Braathen, G. O., Hannigan, J. W., Lambert, J. C., Leblanc, T., McGee, T. J., Nedoluha, G., Petropavlovskikh, I., Seckmeyer, G., Simon, P. C., Steinbrecht, W., & Strahan, S. E. (2018). The network for the detection of atmospheric composition change (NDACC): History, status and perspectives <https://doi.org/10.5194/acp-18-4935-2018>. *Atmospheric Chemistry and Physics*, *18*(7), 4935–4964.

Denning, A. S., Fung, I. Y., & Randall, D. A. (1995). Latitudinal gradient of atmospheric CO2 due to seasonal exchange with land biota. *Nature*, *376*, 240–243.

Dolman, A. J., Noilhan, J., Durand, P., Sarrat, C., Brut, A., Piguet, B., Butet, A., Jarosz, N., Brunet, Y., Loustau, D., Lamaud, E., Tolk, L., Ronda, R., Miglietta, F., Gioli, B., Magliulo, E., Esposito, M.-P., Gerbig, C., Körner, S., . . . Béziat, P.

(2006). The CarboEurope regional experiment strategy <https://doi.org/10.1175/bams-87-10-1367>. *Bulletin of the American Meteorological Society*, *87*(10), 1367–1379.

Dutton, E. G., & Christy, J. R. (1992). Solar radiative forcing at selected locations and evidence for global lower tropospheric cooling following the eruptions of El Chichón and Pinatubo <https://doi.org/10.1029/92GL02495>. *Geophysical Research Letters*, *19*(23), 2313–2316.

Eldering, A., Taylor, T. E., O'Dell, C. W., & Pavlick, R. (2019). The OCO-3 mission: Measurement objectives and expected performance based on 1 year of simulated data <https://doi.org/10.5194/amt-12-2341-2019>. *Atmospheric Measurement Techniques*, *12*(4), 2341–2370.

Eldering, A., Wennberg, P. O., Crisp, D., Schimel, D. S., Gunson, M. R., Chatterjee, A., Liu, J., Schwandner, F. M., Sun, Y., O'Dell, C. W., Frankenberg, C., Taylor, T., Fisher, B., Osterman, G. B., Wunch, D., Hakkarainen, J., Tamminen, J., & Weir, B. (2017). The orbiting carbon observatory-2 early science investigations of regional carbon dioxide fluxes <https://doi.org/10.1126/science.aam5745>. *Science*, *358*(6360).

Etheridge, D. M., Steele, L. P., Langenfelds, R. L., Francey, R. J., Barnola, J.-M., & Morgan, V. I. (1996). Natural and anthropogenic changes in atmospheric CO2 over the last 1000 years from air in Antarctic ice and firn <https://doi.org/10.1029/95JD03410>. *Journal of Geophysical Research: Atmospheres*, *101*(D2), 4115–4128.

Fan, S.-M., Blaine, T. L., & Sarmiento, J. L. (1999). Terrestrial carbon sink in the northern hemisphere estimated from the atmospheric CO2 difference between Mauna Loa and the South Pole since 1959 <https://doi.org/10.3402/tellusb.v51i5.16499>. *Tellus B: Chemical and Physical Meteorology*, *51*(5), 863–870.

Fan, S.-M., Gloor, M., Mahlman, J., Pacala, S., Sarmiento, J., Takahashi, T., & Tans, P. (1998). A large terrestrial carbon sink in North America implied by atmospheric and oceanic carbon dioxide data and models. *Science*, *282*, 442–446.

Filges, A. (2020). *The IAGOS-Core greenhouse gas package: A CO2, CH4, CO and H2O measurement system for deployment on board commercial airliners*. Friedrich-Schiller-Universität Jena.

Filges, A., Gerbig, C., Chen, H., Franke, H., Klaus, C., & Jordan, A. (2015). The IAGOS-core greenhouse gas package: A measurement system for continuous airborne observations of CO2, CH4, H2O and CO <https://doi.org/10.3402/tellusb.v67.27989>. *Tellus B: Chemical and Physical Meteorology*, *67*(1), 27989.

Fonselius, S. (1958). Map and coordinates of the chemical and CO2 stations western Europe. *Tellus*, *10*(1), 170–171.

Frey, M., Hase, F., Blumenstock, T., Gross, J., Kiel, M., Tsidu, G. M., Schafer, K., Sha, M. K., & Orphal, J. (2015). Calibration and instrumental line shape characterization of a set of portable FTIR spectrometers for detecting greenhouse gas emissions <https://doi.org/10.5194/amt-8-3047-2015>. *Atmospheric Measurement Techniques*, *8*(7), 3047–3057.

Frey, M., Sha, M., Hase, F., Kiel, M., Blumenstock, T., Harig, R., Surawicz, G., Deutscher, N., Shiomi, K., Franklin, J., Bösch, H., Chen, J., Grutter, M., Ohyama, H., Sun, Y., Butz, A., Mengistu Tsidu, G., Ene, D., Wunch, D., . . . Orphal, J. (2019). Building the COllaborative Carbon Column Observing Network (COCCON): Long-term stability and ensemble performance of the EM27/SUN Fourier transform spectrometer <https://doi.org/10.5194/amt-12-1513-2019>. *Atmospheric Measurement Techniques*, *12*(3), 1513–1530.

Frey, M. M., Hase, F., Blumenstock, T., Dubravica, D., Groß, J., Göttsche, F., Handjaba, M., Amadhila, P., Mushi, R., Morino, I., Shiomi, K., Sha, M. K., de Mazière, M., & Pollard, D. F. (2021). Long-term column-averaged greenhouse gas observations using a COCCON spectrometer at the high-surface-albedo site in Gobabeb, Namibia <https://doi.org/10.5194/amt-14-5887-2021>. *Atmospheric Measurement Techniques*, *14*(9), 5887–5911.

Friedlingstein, P., Jones, M. W., O'Sullivan, M., Andrew, R. M., Bakker, D. C. E., Hauck, J., Le Quéré, C., Peters, G. P., Peters, W., Pongratz, J., Sitch, S., Canadell, J. G., Ciais, P., Jackson, R. B., Alin, S. R., Anthoni, P., Bates, N. R., Becker, M., Bellouin, N., . . . Zeng, J. (2022). Global carbon budget 2021 <https://essd.copernicus.org/articles/14/1917/2022/>. *Earth System Science Data*, *14*(4), 1917–2005.

From, E., & Keeling, C. D. (1986). Reassessment of late 19th century atmospheric carbon dioxide variations in the air of western Europe and the British Isles based on an unpublished analysis of contemporary air masses by G. S. Callendar <https://doi.org/10.1111/j.1600-0889.1986.tb00092.x>. *Tellus B*, *38B*(2), 87–105.

Fung, I. Y., Prenctice, K., Matthews, E., Lerner, J., & Russell, G. (1983). Three-dimensional tracer model study of atmospheric CO2: Response to seasonal exchanges with the terrestrial biosphere. *Journal of Geophysical Research*, *88*(C2), 1281–1294.

Gatti, L. V., Basso, L. S., Miller, J. B., Gloor, M., Gatti Domingues, L., Cassol, H. L. G., Tejada, G., Aragão, L. E. O. C., Nobre, C., Peters, W., Marani, L., Arai, E., Sanches, A. H., Corrêa, S. M., Anderson, L., Von Randow, C., Correia, C. S. C., Crispim, S. P., & Neves, R. A. L. (2021). Amazonia as a carbon source linked to deforestation and climate change <https://doi.org/10.1038/s41586-021-03629-6>. *Nature*, 595(7867), 388–393.

Gatti, L. V., Miller, J. B., D'amelio, M. T. S., Martinewski, A., Basso, L. S., Gloor, M. E., Wofsy, S., & Tans, P. (2010). Vertical profiles of CO2 above eastern Amazonia suggest a net carbon flux to the atmosphere and balanced biosphere between 2000 and 2009 <https://doi.org/10.1111/j.1600-0889.2010.00484.x>. *Tellus B: Chemical and Physical Meteorology*, *62*(5), 581–594.

Gaudry, A., Monfray, P., Polian, G., & Lambert, G. (1987). The 1982–83 El-Niño: A 6 billion ton CO2 release. *Tellus*, *39B*, 209–213.

Gerbig, C., Lin, J. C., Wofsy, S. C., Daube, B. C., Andrews, A. E., Stephens, B. B., Bakwin, P. S., & Grainger, C. A. (2003). Toward constraining regional-scale fluxes of CO2 with atmospheric observations over a continent: 1. Observed spatial variability from airborne platforms <https://doi.org/10.1029/2002JD003018>. *Journal of Geophysical Research-Atmospheres*, *108*(D24).

González del Castillo, E., Taquet, N., Bezanilla, A., Stremme, W., Ramonet, M., Laurent, O., Yang Xu, Y., Delmotte, M., & Michel Grutter, M. (2021). CO2 variability in the Mexico City region from in situ measurements at an urban and a background site <https://doi.org/10.20937/ATM.52956>. *Atmosfera*, *35*(2), 377–393.

Graven, H., Allison, C. E., Etheridge, D. M., Hammer, S., Keeling, R. F., Levin, I., Meijer, H. A. J., Rubino, M., Tans, P. P., Trudinger, C. M., Vaughn, B. H., & White, J. W. C. (2017). Compiled records of carbon isotopes in atmospheric CO2 for historical simulations in CMIP6 <https://doi.org/10.5194/gmd-10-4405-2017>. *Geoscientific Model Development*, *10*(12), 4405–4417.

Graven, H. D. (2015). Impact of fossil fuel emissions on atmospheric radiocarbon and various applications of radiocarbon over this century <https://doi.org/10.1073/pnas.1504467112>. *Proceedings of the National Academy of Sciences*, *112*(31), 9542–9545.

Graven, H. D., Keeling, R. F., Piper, S. C., Patra, P. K., Stephens, B. B., Wofsy, S. C., Welp, L. R., Sweeney, C., Tans, P. P., Kelley, J. J., Daube, B. C., Kort, E. A., Santoni, G. W., & Bent, J. D. (2013). Enhanced seasonal exchange of CO2 by northern ecosystems since 1960 <https://doi.org/10.1126/science.1239207>. *Science*, *341*(6150), 1085–1089.

Guerlet, S., Basu, S., Butz, A., Krol, M., Hahne, P., Houweling, S., Hasekamp, O. P., & Aben, I. (2013). Reduced carbon uptake during the 2010 Northern Hemisphere summer from GOSAT <https://doi.org/10.1002/grl.50402>. *Geophysical Research Letters*, *40*(10), 2378–2383.

Gurney, K. R., Baker, D., Rayner, P., & Denning, S. (2008). Interannual variations in continental-scale net carbon exchange and sensitivity to observing networks estimated from atmospheric CO2 inversions for the period 1980 to 2005. *Global Biogeochemical Cycles*, *22*(3).

Hall, T. M., Waugh, D. W., Boering, K. A., & Plumb, R. A. (1999). Evaluation of transport in stratospheric models <https://doi.org/10.1029/1999JD900226>. *Journal of Geophysical Research: Atmospheres*, *104*(D15), 18815–18839.

Hase, F., Drouin, B. J., Roehl, C. M., Toon, G. C., Wennberg, P. O., Wunch, D., Blumenstock, T., Desmet, F., Feist, D. G., Heikkinen, P., De Mazière, M., Rettinger, M., Robinson, J., Schneider, M., Sherlock, V., Sussmann, R., Té, Y., Warneke, T., & Weinzierl, C. (2013). Calibration of sealed HCl cells used for TCCON instrumental line shape monitoring <https://doi.org/10.5194/amt-6-3527-2013>. *Atmospheric Measurement Techniques*, *6*(12), 3527–3537.

Hase, F., Frey, M., Blumenstock, T., Gross, J., Kiel, M., Kohlhepp, R., Tsidu, G. M., Schafer, K., Sha, M. K., & Orphal, J. (2015). Application of portable FTIR spectrometers for detecting greenhouse gas emissions of the major city Berlin <https://doi.org/10.5194/amt-8-3059-2015>. *Atmospheric Measurement Techniques*, *8*(7), 3059–3068.

Heimann, M., Keeling, C. D., & Fung, I. (1986). Simulating the atmospheric carbon dioxide distribution with a three-dimensional tracer model. In J. R. Trabalka & D. E. Reichle (Eds.), *The changing carbon cycle* (pp. 16–49). Springer-Verlag.

Heiskanen, J., Brümmer, C., Buchmann, N., Calfapietra, C., Chen, H., Gielen, B., Gkritzalis, T., Hammer, S., Hartman, S., Herbst, M., Janssens, I. A., Jordan, A., Juurola, E., Karstens, U., Kasurinen, V., Kruijt, B., Lankreijer, H., Levin, I., Linderson, M.-L., . . . Kutsch, W. (2022). The integrated carbon observation system in Europe <https://doi.org/10.1175/bams-d-19-0364.1>. *Bulletin of the American Meteorological Society*, *103*(3), E855–E872.

Hooghiem, J. J. D., Popa, M. E., Röckmann, T., Grooß, J. U., Tritscher, I., Müller, R., Kivi, R., & Chen, H. (2020). Wildfire smoke in the lower stratosphere identified by in situ CO observations <https://doi.org/10.5194/acp-20-13985-2020>. *Atmospheric Chemistry and Physics*, *20*(22), 13985–14003.

Houweling, S., Breon, F. M., Aben, I., Rödenbeck, C., Gloor, M., Heimann, M., & Ciais, P. (2004). Inverse modeling of CO2 sources and sinks using satellite data: A synthetic inter-comparison of measurement techniques and their performance as a function of space and time <https://doi.org/10.5194/acp-4-523-2004>. *Atmospheric Chemistry and Physics*, *4*(2), 523–538.

Hungershoefer, K., Breon, F. M., Peylin, P., Chevallier, F., Rayner, P., Klonecki, A., Houweling, S., & Marshall, J. (2010). Evaluation of various observing systems for the global monitoring of CO2 surface fluxes <https://doi.org/10.5194/acp-10-10503-2010>. *Atmospheric Chemistry and Physics*, *10*(21), 10503–10520.

Integrated Carbon Observation System – Research Infrastructure (ICOS-RI). (2020). *ICOS atmosphere station specifications V2.0 Report edited by O. Laurent, ICOS-RI*.

Inoue, M., Morino, I., Uchino, O., Miyamoto, Y., Yoshida, Y., Yokota, T., Machida, T., Sawa, Y., Matsueda, H., Sweeney, C., Tans, P. P., Andrews, A. E., Biraud, S. C., Tanaka, T., Kawakami, S., & Patra, P. K. (2013). Validation of XCO2 derived from SWIR spectra of GOSAT TANSO-FTS with aircraft measurement data <https://doi.org/10.5194/acp-13-9771-2013>. *Atmospheric Chemistry and Physics*, *13*(19), 9771–9788.

Janssens-Maenhout, G., Pinty, B., Dowell, M., Zunker, H., Andersson, E., Balsamo, G., Bézy, J. L., Brunhes, T., Bösch, H., Bojkov, B., Brunner, D., Buchwitz, M., Crisp, D., Ciais, P., Counet, P., Dee, D., Denier van der Gon, H., Dolman, H., Drinkwater, M. R., . . . Veefkind, P. (2020). Toward an operational anthropogenic CO2 emissions monitoring and verification support capacity <https://doi.org/10.1175/BAMS-D-19-0017.1>. *Bulletin of the American Meteorological Society*, *101*(8), E1439–E1451.

Johnston, H. (1989). Evaluation of excess carbon 14 and strontium 90 data for suitability to test two-dimensional stratospheric models <https://doi.org/10.1029/JD094iD15p18485>. *Journal of Geophysical Research: Atmospheres*, *94*(D15), 18485–18493.

Jones, C. D., & Friedlingstein, P. (2020). Quantifying process-level uncertainty contributions to TCRE and carbon budgets for meeting Paris agreement climate targets <https://doi.org/10.1088/1748-9326/ab858a>. *Environmental Research Letters*, *15*(7), 074019.

Karion, A., Sweeney, C., Kort, E. A., Shepson, P. B., Brewer, A., Cambaliza, M., Conley, S. A., Davis, K., Deng, A., Hardesty, M., Herndon, S. C., Lauvaux, T., Lavoie, T., Lyon, D., Newberger, T., Pétron, G., Rella, C., Smith, M., Wolter, S., . . . Tans, P. (2015). Aircraft-based estimate of Total methane emissions from the Barnett shale region <https://doi.org/10.1021/acs.est.5b00217>. *Environmental Science & Technology*, *49*(13), 8124–8131.

Karion, A., Sweeney, C., Tans, P., & Newberger, T. (2010). AirCore: An innovative atmospheric sampling system. *Journal of Atmospheric and Oceanic Technology*, *27*(11), 1839–1853.

Karion, A., Sweeney, C., Wolter, S., Newberger, T., Chen, H., Andrews, A., Kofler, J., Neff, D., & Tans, P. (2013). Long-term greenhouse gas measurements from aircraft <https://doi.org/10.5194/amt-6-511-2013>. *Atmospheric Measurement Techniques*, *6*(3), 511–526.

Kaufmann, M., Gusev, O. A., Grossmann, K. U., Roble, R. G., Hagan, M. E., Hartsough, C., & Kutepov, A. A. (2002). The vertical and horizontal distribution of CO2 densities in the upper mesosphere and lower thermosphere as measured by CRISTA <https://doi.org/10.1029/2001JD000704>. *Journal of Geophysical Research: Atmospheres*, *107*(D23), CRI 10-11–CRI 10-19.

Keeling, C. D. (1960). The concentration and isotopic abundance of carbon dioxide in the atmosphere. *Tellus*, *12*, 200–203.

Keeling, C. D., Chin, J. F. S., & Whorf, T. P. (1996). Increased activity of northern vegetation inferred from atmospheric CO2 measurements. *Nature*, *382*, 146–149.

Keeling, C. D., Harris, T. B., & Wilkins, E. M. (1968). Concentration of atmospheric carbon dioxide at 500 and 700 millibars <https://doi.org/10.1029/JB073i014p04511>. *Journal of Geophysical Research (1896–1977)*, *73*(14), 4511–4528.

Keeling, C. D., Piper, S. C., Bacastow, R. B., Wahlen, M., Whorf, T. P., Heimann, M., & Meijer, H. A. (2001). *Exchanges of atmospheric CO2 and 13CO2 with the terrestrial biosphere and oceans from 1978 to 2000*. Report N° 01-06, 88 pages pp, edited by Scripps Institution of Oceanography Reference Series, San Diego, USA.

Keeling, C. D., Piper, S. C., & Heimann, M. (1989). A three-dimensional model of atmospheric CO_2 transport based on observed winds, 4, mean annual gradients and interannual variations. In D. H. Peterson (Ed.). *Aspects of climate variability in the Pacific and Western Americas* (Geophysical Monogr. Ser). American Geophysical Union.

Keeling, C. D., & Rakestraw, N. W. (1960). The concentration of carbon dioxide in the atmosphere. *Journal of Geophysical Research*, *65*(8), 2502.

Keeling, C. D., & Revelle, R. (1985). Effects of EL Nino/Southern Oscillation on the atmospheric content of carbon dioxide. *Meteoritics*, *20*, 437.

Keeling, R. F., & Graven, H. D. (2021). Insights from time series of atmospheric carbon dioxide and related tracers <https://doi.org/10.1146/annurev-environ-012220-125406>. *Annual Review of Environment and Resources*, *46*(1), 85–110.

Kiel, M., Eldering, A., Roten, D. D., Lin, J. C., Feng, S., Lei, R., Lauvaux, T., Oda, T., Roehl, C. M., Blavier, J.-F., & Iraci, L. T. (2021). Urban-focused satellite CO2 observations from the orbiting carbon Observatory-3: A first look at the Los Angeles megacity <https://doi.org/10.1016/j.rse.2021.112314>. *Remote Sensing of Environment*, *258*, 112314.

Kim, J.-S., Kug, J.-S., Yoon, J.-H., & Jeong, S.-J. (2016). Increased atmospheric CO2 growth rate during El Niño driven by reduced terrestrial productivity in the CMIP5 ESMs <https://doi.org/10.1175/JCLI-D-14-00672.1>. *Journal of Climate*, *29*(24), 8783–8805.

Kjellström, E., Feichter, J., & Hoffman, G. (2000). Transport of SF6 and 14CO2 in the atmospheric general circulation model ECHAM4 <https://doi.org/10.1034/j.1600-0889.2000.00882.x>. *Tellus B*, *52*(1), 1–18.

Klausner, T., Mertens, M., Huntrieser, H., Galkowski, M., Kuhlmann, G., Baumann, R., Fiehn, A., Jöckel, P., Pühl, M., & Roiger, A. (2020). Urban greenhouse gas emissions from the Berlin area: A case study using airborne CO2 and CH4 in situ observations in summer 2018 <https://doi.org/10.1525/elementa.411>. *Elementa: Science of the Anthropocene*, *8*, 15.

Knapp, M., Kleinschek, R., Hase, F., Agustí-Panareda, A., Inness, A., Barré, J., Landgraf, J., Borsdorff, T., Kinne, S., & Butz, A. (2021). Shipborne measurements of XCO2, XCH4, and XCO above the Pacific Ocean and comparison to CAMS atmospheric analyses and S5P/TROPOMI <https://doi.org/10.5194/essd-13-199-2021>. *Earth System Science Data*, *13*(1), 199–211.

Knorr, W. (2009). Is the airborne fraction of anthropogenic CO2 emissions increasing? <https://doi.org/10.1029/2009GL040613> *Geophysical Research Letters*, *36*(21).

Kovaltsov, G. A., Mishev, A., & Usoskin, I. G. (2012). A new model of cosmogenic production of radiocarbon 14C in the atmosphere <https://doi.org/10.1016/j.epsl.2012.05.036>. *Earth and Planetary Science Letters*, *337–338*, 114–120.

Kozlova, E. A., Manning, A. C., Kisilyakhov, Y., Seifert, T., & Heimann, M. (2008). Seasonal, synoptic, and diurnal-scale variability of biogeochemical trace gases and O-2 from a 300-m tall tower in Central Siberia. *Global Biogeochemical Cycles*, *22*(4).

Landschützer, P., Gruber, N., Haumann, F. A., Rödenbeck, C., Bakker, D. C. E., van Heuven, S., Hoppema, M., Metzl, N., Sweeney, C., Takahashi, T., Tilbrook, B., & Wanninkhof, R. (2015). The reinvigoration of the Southern Ocean carbon sink <https://doi.org/10.1126/science.aab2620>. *Science*, *349*(6253), 1221–1224.

Lauvaux, T., Gurney, K. R., Miles, N. L., Davis, K. J., Richardson, S. J., Deng, A., Nathan, B. J., Oda, T., Wang, J. A., Hutyra, L., & Turnbull, J. (2020). Policy-relevant assessment of urban CO2 emissions <https://doi.org/10.1021/acs.est.0c00343>. *Environmental Science & Technology*, *54*(16), 10237–10245.

Lauvaux, T., Schuh, A. E., Bocquet, M., Wu, L., Richardson, S., Miles, N., & Davis, K. J. (2012). Network design for mesoscale inversions of CO2 sources and sinks <https://doi.org/10.3402/tellusb.v64i0.17980>. *Tellus B: Chemical and Physical Meteorology*, *64*(1), 17980.

Lauvaux, T., Uliasz, M., Sarrat, C., Chevallier, F., Bousquet, P., Lac, C., Davis, K. J., Ciais, P., Denning, A. S., & Rayner, P. J. (2008). Mesoscale inversion: First results from the CERES campaign with synthetic data. *Atmospheric Chemistry and Physics*, *8*(13), 3459–3471.

Le Quéré, C., Jackson, R. B., Jones, M. W., Smith, A. J. P., Abernethy, S., Andrew, R. M., De-Gol, A. J., Willis, D. R., Shan, Y., Canadell, J. G., Friedlingstein, P., Creutzig, F., & Peters, G. P. (2020). Temporary reduction in daily global CO2 emissions during the COVID-19 forced confinement <https://doi.org/10.1038/s41558-020-0797-x>. *Nature Climate Change*, *10*(7), 647–653.

Le Quéré, C., Rödenbeck, C., Buitenhuis, E. T., Conway, T. J., Langenfelds, R., Gomez, A., Labuschagne, C., Ramonet, M., Nakazawa, T., Metzl, N., Gillett, N., & Heimann, M. (2007). Saturation of the Southern Ocean CO2 sink due to recent climate change <https://doi.org/10.1126/science.1136188>. *Science*, *316*(5832), 1735–1738.

Levin, I., Ciais, P., Langenfelds, R., Schmidt, M., Ramonet, M., Sidorov, K., Tchebakova, N., Gloor, M., Heimann, M., Schulze, E.-D., Vygodskaya, N., Shibistova, O., & Lloyd, J. (2002). Three years of trace gas observations over the EuroSiberian domain derived from aircraft sampling—A concerted action <https://doi.org/10.3402/tellusb.v54i5.16717>. *Tellus B—Chemical and Physical Meteorology*, *54*(5), 696–712.

Levin, I., Graul, R., & Trivett, N. B. A. (1995). Long-term observations of atmospheric CO2 and carbon isotopes at continental sites in Germany <https://doi.org/10.3402/tellusb.v47i1-2.15996>. *Tellus B: Chemical and Physical Meteorology*, *47*(1–2), 23–34.

Levin, I., Hammer, S., Kromer, B., Preunkert, S., Weller, R., & Worthy, D. E. (2022). Radiocarbon in global tropospheric carbon dioxide <https://doi.org/10.1017/RDC.2021.102>. *Radiocarbon*, *64*(4), 781–791.

Levin, I., Kromer, B., Schoch-Fischer, H., Bruns, M., Münnich, M., Berdau, D., Vogel, J. C., & Münnich, K. O. (1985). 25 years of tropospheric 14C observations in Central Europe <https://doi.org/10.1017/S0033822200006895>. *Radiocarbon*, *27*(1), 1–19.

Levin, I., Naegler, T., Kromer, B., Diehl, M., Francey, R., Gomez-Pelaez, A., Steele, P., Wagenbach, D., Weller, R., & Worthy, D. (2010). Observations and modelling of the global distribution and long-term trend of atmospheric 14CO2 <https://doi.org/10.1111/j.1600-0889.2009.00446.x>. *Tellus B: Chemical and Physical Meteorology*, *62*(1), 26–46.

Lian, J., Lauvaux, T., Utard, H., Bréon, F.-M., Broquet, G., Ramonet, M., Laurent, O., Albarus, I., Cucchi, K., & Ciais, P. (2022). Assessing the effectiveness of an Urban CO2 monitoring network over the Paris Region through the COVID-19 lockdown natural experiment. *Environmental Science & Technology*, *56*(4), 2153–2162.

Libby, W. F. (1956). Radioactive fallout and radioactive strontium. *Science*, *123*(3199), 657–660.

Lingenfelter, R. E. (1963). Production of carbon 14 by cosmic-ray neutrons <https://doi.org/10.1029/RG001i001p00035>. *Reviews of Geophysics*, *1*(1), 35–55.

Liu, J., Bowman, K. W., Schimel, D. S., Parazoo, N. C., Jiang, Z., Lee, M., Bloom, A. A., Wunch, D., Frankenberg, C., Sun, Y., O'Dell, C. W., Gurney, K. R., Menemenlis, D., Gierach, M., Crisp, D., & Eldering, A. (2017). Contrasting carbon cycle responses of the tropical continents to the 2015–2016 El Niño <https://doi.org/10.1126/science.aam5690>. *Science*, *358*(6360).

Liu, Z., Ciais, P., Deng, Z., Lei, R., Davis, S. J., Feng, S., Zheng, B., Cui, D., Dou, X., Zhu, B., Guo, R., Ke, P., Sun, T., Lu, C., He, P., Wang, Y., Yue, X., Wang, Y., Lei, Y., . . . Schellnhuber, H. J. (2020). Near-real-time monitoring of global CO2 emissions reveals the effects of the COVID-19 pandemic <https://doi.org/10.1038/s41467-020-18922-7>. *Nature Communications*, *11*(1), 5172.

Long, M. C., Stephens, B. B., McKain, K., Sweeney, C., Keeling, R. F., Kort, E. A., Morgan, E. J., Bent, J. D., Chandra, N., Chevallier, F., Commane, R., Daube, B. C., Krummel, P. B., Loh, Z., Luijkx, I. T., Munro, D., Patra, P., Peters, W., Ramonet, M., . . . Wofsy, S. C. (2021). Strong Southern Ocean carbon uptake evident in airborne observations <https://doi.org/10.1126/science.abi4355>. *Science*, *374*(6572), 1275–1280.

Lopez, M., Schmidt, M., Ramonet, M., Bonne, J. L., Colomb, A., Kazan, V., Laj, P., & Pichon, J. M. (2015). Three years of semicontinuous greenhouse gas measurements at the Puy de Dôme station (Central France) <https://doi.org/10.5194/amt-8-3941-2015>. *Atmospheric Measurement Techniques*, *8*, 3941–3958.

Lucht, W., Prentice, I. C., Myneni, R. B., Sitch, S., Friedlingstein, P., Cramer, W., Bousquet, P., Buermann, W., & Smith, B. (2002). Climatic control of the high-latitude vegetation greening trend and Pinatubo effect <https://doi.org/10.1126/science.1071828>. *Science*, *296*(5573), 1687–1689.

Machida, T., Matsueda, H., Sawa, Y., Nakagawa, Y., Hirotani, K., Kondo, N., Goto, K., Nakazawa, T., Ishikawa, K., & Ogawa, T. (2008). Worldwide measurements of atmospheric CO2 and other trace gas species using commercial airlines <https://doi.org/10.1175/2008jtecha1082.1>. *Journal of Atmospheric and Oceanic Technology*, *25*(10), 1744–1754.

Maksyutov, S., Takagi, H., Valsala, V. K., Saito, M., Oda, T., Saeki, T., Belikov, D. A., Saito, R., Ito, A., Yoshida, Y., Morino, I., Uchino, O., Andres, R. J., & Yokota, T. (2013). Regional CO2 flux estimates for 2009–2010 based on GOSAT and ground-based CO2 observations <https://doi.org/10.5194/acp-13-9351-2013>. *Atmospheric Chemistry and Physics*, *13*(18), 9351–9373.

van Marle, M. J. E., van Wees, D., Houghton, R. A., Field, R. D., Verbesselt, J., & van der Werf, G. R. (2022). New land-use-change emissions indicate a declining CO2 airborne fraction <https://doi.org/10.1038/s41586-021-04376-4>. *Nature*, *603*(7901), 450–454.

Matsueda, H., Machida, T., Sawa, Y., Nakagawa, Y., Hirotani, K., Ikeda, H., Kondo, N., & Goto, K. (2008). Evaluation of atmospheric CO2 measurements from new flask air sampling of JAL airliner observations <https://doi.org/10.2467/mripapers.59.1>. *Papers in Meteorology and Geophysics*, *59*, 1–17.

Mazurenka, M., Orr-Ewing, A. J., Peverall, R., & Ritchie, G. A. D. (2005). 4 Cavity ring-down and cavity enhanced spectroscopy using diode lasers <https://doi.org/10.1039/B408909J>. *Annual Reports Section "C" (Physical Chemistry)*, *101*, 100–142.

Miles, N. L., Richardson, S. J., Davis, K. J., Lauvaux, T., Andrews, A. E., West, T. O., Bandaru, V., & Crosson, E. R. (2012). Large amplitude spatial and temporal gradients in atmospheric boundary layer CO2mole fractions detected with a tower-based network in the U.S. upper Midwest <https://doi.org/10.1029/2011JG001781>. *Journal of Geophysical Research: Biogeosciences*, *117*(G1).

Miller, J. B., Lehman, S. J., Verhulst, K. R., Miller, C. E., Duren, R. M., Yadav, V., Newman, S., & Sloop, C. D. (2020). Large and seasonally varying biospheric CO2 fluxes in the Los Angeles megacity revealed by atmospheric radiocarbon <https://doi.org/10.1073/pnas.2005253117>. *Proceedings of the National Academy of Sciences*, *117*(43), 26681–26687.

Müller, A., Tanimoto, H., Sugita, T., Machida, T., Nakaoka, S., Patra, P. K., Laughner, J., & Crisp, D. (2021). New approach to evaluate satellite-derived XCO2 over oceans by integrating ship and aircraft observations <https://doi.org/10.5194/acp-21-8255-2021>. *Atmospheric Chemistry and Physics*, *21*(10), 8255–8271.

Münnich, K., & Vogel, J. (1963). *Investigations of meridional transport in the troposphere by means of radiocarbon measurements* [Paper presented]. IAEA Vienna, Vienna, Austria.

Nassar, R., Moeini, O., Mastrogiacomo, J.-P., O'Dell, C. W., Nelson, R. R., Kiel, M., Chatterjee, A., Eldering, A., & Crisp, D. (2022). Tracking CO2 emission reductions from space: A case study at Europe's largest fossil fuel power plant. *Frontiers in Remote Sensing*, 3.

Noël, S., Reuter, M., Buchwitz, M., Borchardt, J., Hilker, M., Bovensmann, H., Burrows, J. P., Di Noia, A., Suto, H., Yoshida, Y., Buschmann, M., Deutscher, N. M., Feist, D. G., Griffith, D. W. T., Hase, F., Kivi, R., Morino, I., Notholt, J., Ohyama, H., . . . Warneke, T. (2021). XCO2 retrieval for GOSAT and GOSAT-2 based on the FOCAL algorithm <https://doi.org/10.5194/amt-14-3837-2021>. *Atmospheric Measurement Techniques*, *14*(5), 3837–3869.

O'Brien, D. M., & Rayner, P. J. (2002). Global observations of the carbon budget, 2, CO2 column from differential absorption of reflected sunlight in the 1.61 μm band of CO2 <https://doi.org/10.1029/2001JD000617>. *Journal of Geophysical Research: Atmospheres*, *107*(D18), ACH 6-1–ACH 6-16.

O'Dell, C. W., Connor, B., Bösch, H., O'Brien, D., Frankenberg, C., Castano, R., Christi, M., Eldering, D., Fisher, B., Gunson, M., McDuffie, J., Miller, C. E., Natraj, V., Oyafuso, F., Polonsky, I., Smyth, M., Taylor, T., Toon, G. C., Wennberg, P. O., & Wunch, D. (2012). The ACOS CO2 retrieval algorithm—Part 1: Description and validation against synthetic observations <https://doi.org/10.5194/amt-5-99-2012>. *Atmospheric Measurement Techniques*, *5*(1), 99–121.

O'Dell, C. W., Eldering, A., Wennberg, P. O., Crisp, D., Gunson, M. R., Fisher, B., Frankenberg, C., Kiel, M., Lindqvist, H., Mandrake, L., Merrelli, A., Natraj, V., Nelson, R. R., Osterman, G. B., Payne, V. H., Taylor, T. E., Wunch, D., Drouin, B. J., Oyafuso, F., . . . Velazco, V. A. (2018). Improved retrievals of carbon dioxide from orbiting carbon observatory-2 with the version 8 ACOS algorithm <https://doi.org/10.5194/amt-11-6539-2018>. *Atmospheric Measurement Techniques*, *11*(12), 6539–6576.

Okada, K., Okada, N., Takagi, K., Urano, S.-I., Nishida, Y., Aguilos, M., & Kobayashi, T. (2012). CO2 flux estimation for a valley terrain using the atmospheric boundary layer method <https://doi.org/10.2480/agrmet.68.3.1>. *Journal of Agricultural Meteorology*, *68*(3), 165–174.

Palmer, P. I., O'Doherty, S., Allen, G., Bower, K., Bösch, H., Chipperfield, M. P., Connors, S., Dhomse, S., Feng, L., Finch, D. P., Gallagher, M. W., Gloor, E., Gonzi, S., Harris, N. R. P., Helfter, C., Humpage, N., Kerridge, B., Knappett, D., Jones, R. L., . . . Young, D. (2018). A measurement-based verification framework for UK greenhouse gas emissions: An overview

of the Greenhouse gAs UK and Global Emissions (GAUGE) project <https://doi.org/10.5194/acp-18-11753-2018>. *Atmospheric Chemistry and Physics*, *18*(16), 11753–11777.

Park, H., Jeong, S., Park, H., Labzovskii, L. D., & Bowman, K. W. (2021). An assessment of emission characteristics of Northern Hemisphere cities using spaceborne observations of CO2, CO, and NO2 <https://doi.org/10.1016/j.rse.2020.112246>. *Remote Sensing of Environment*, *254*, 112246.

Peiro, H., Crowell, S., Schuh, A., Baker, D. F., O'Dell, C., Jacobson, A. R., Chevallier, F., Liu, J., Eldering, A., Crisp, D., Deng, F., Weir, B., Basu, S., Johnson, M. S., Philip, S., & Baker, I. (2022). Four years of global carbon cycle observed from the Orbiting Carbon Observatory 2 (OCO-2) version 9 and in situ data and comparison to OCO-2 version 7 <https://doi.org/10.5194/acp-22-1097-2022>. *Atmospheric Chemistry and Physics*, *22*(2), 1097–1130.

Petit, J. R., & Raynaud, D. (2020). Forty years of ice-core records of CO2 <https://doi.org/10.1038/d41586-020-00809-8>. *Nature*, *579*, 505–506.

Philip, S., Johnson, M. S., Baker, D. F., Basu, S., Tiwari, Y. K., Indira, N. K., Ramonet, M., & Poulter, B. (2022). OCO-2 satellite-imposed constraints on terrestrial biospheric CO2 fluxes over South Asia <https://doi.org/10.1029/2021JD035035>. *Journal of Geophysical Research: Atmospheres*, *127*(3), e2021JD035035.

Pitt, J. R., Allen, G., Bauguitte, S. J. B., Gallagher, M. W., Lee, J. D., Drysdale, W., Nelson, B., Manning, A. J., & Palmer, P. I. (2019). Assessing London CO2, CH4 and CO emissions using aircraft measurements and dispersion modelling <https://doi.org/10.5194/acp-19-8931-2019>. *Atmospheric Chemistry and Physics*, *19*(13), 8931–8945.

Rafter, T. A., & Fergusson, G. J. (1957). Atom bomb effect—Recent increase of carbon-14 content of the atmosphere and biosphere <https://doi.org/10.1126/science.126.3273.557>. *Science*, *126*(3273), 557–558.

Ramonet, M., Ciais, P., Apadula, F., Bartyzel, J., Bastos, A., Bergamaschi, P., Blanc, P.-É., Brunner, D., Torchiarolo, L. C. D., Calzolari, F., Chen, H., Chmura, L., Colomb, A., Conil, S., Cristofanelli, P., Cuevas, E., Curcoll, R., Delmotte, M., Sarra, A. D., . . . Kwok, C. Y. (2020). The fingerprint of the summer 2018 drought in Europe on ground-based atmospheric CO2 measurements <https://doi.org/10.1098/rstb.2019.0513>. *Philosophical Transactions of the Royal Society B: Biological Sciences*, *375*(1810), 20190513.

Ramonet, M., Ciais, P., Nepomniachii, I., Sidorov, K., Neubert, R., Langendörfer, U., Picard, D., Kazan, V., Biraud, S., Gusti, M., Kolle, O., Schulze, E.-D., & Lloyd, J. (2002). Three years of aircraft-based trace gas measurements over the Fyodorovskoye southern taiga forest, 300 km north-west of Moscow <https://doi.org/10.3402/tellusb.v54i5.16720>. *Tellus B—Chemical and Physical Meteorology*, *54*(5), 713–734.

Ramonet, M., & Monfray, P. (1996). CO2 baseline concept in 3-D atmospheric transport models <https://doi.org/10.3402/tellusb.v48i4.15929>. *Tellus B—Chemical and Physical Meteorology*, *48*(4), 502–520.

Rastogi, B., Miller, J. B., Trudeau, M., Andrews, A. E., Hu, L., Mountain, M., Nehrkorn, T., Baier, B., McKain, K., Mund, J., Guan, K., & Alden, C. B. (2021). Evaluating consistency between total column CO2 retrievals from OCO-2 and the in situ network over North America: Implications for carbon flux estimation <https://doi.org/10.5194/acp-21-14385-2021>. *Atmospheric Chemistry and Physics*, 21(18), 14385–14401.

Raynaud, D., Chowdhry Beeman, J., Chappellaz, J., Parrenin, F., & Shin, J. (2020). Antarctic air bubbles and the long-term ice core record of CO2 and other greenhouse gases <https://doi.org/10.1016/B978-0-12-817925-3.00002-1>. In M. Oliva & J. Ruiz-Fernández (Eds.), *Past Antarctica* (pp. 27–50). Academic Press.

Rayner, P. J., & O'Brien, D. M. (2001). The utility of remotely sensed CO2 concentration data in surface source inversions (vol 28, pg 175, 2001). *Geophysical Research Letters*, *28*(12), 2429.

Rella, C. W., Chen, H., Andrews, A. E., Filges, A., Gerbig, C., Hatakka, J., Karion, A., Miles, N. L., Richardson, S. J., Steinbacher, M., Sweeney, C., Wastine, B., & Zellweger, C. (2013). High accuracy measurements of dry mole fractions of carbon dioxide and methane in humid air <https://doi.org/10.5194/amt-6-837-2013>. *Atmospheric Measurement Techniques*, *6*(3), 837–860.

Rödenbeck, C., Zaehle, S., Keeling, R., & Heimann, M. (2018). History of El Nino impacts on the global carbon cycle 1957–2017: A quantification from atmospheric CO2 data <https://doi.org/10.1098/rstb.2017.0303>. *Philosophical Transactions of the Royal Society B: Biological Sciences*, *373*(1760), 20170303.

Rubino, M., Etheridge, D. M., Thornton, D. P., Howden, R., Allison, C. E., Francey, R. J., Langenfelds, R. L., Steele, L. P., Trudinger, C. M., Spencer, D. A., Curran, M. A. J., van Ommen, T. D., & Smith, A. M. (2019). Revised records of atmospheric trace gases CO2, CH4, N2O, and δ13C-CO2 over the last 2000 years from Law Dome, Antarctica <https://doi.org/10.5194/essd-11-473-2019>. *Earth System Science Data*, *11*(2), 473–492.

Ruckstuhl, A. F., Henne, S., Reimann, S., Steinbacher, M., Vollmer, M. K., O'Doherty, S., Buchmann, B., & Hueglin, C. (2012). Robust extraction of baseline signal of atmospheric trace species using local regression <https://doi.org/10.5194/amt-5-2613-2012>. *Atmospheric Measurement Techniques*, *5*(11), 2613–2624.

Saeki, T., Maksyutov, S., Sasakawa, M., Machida, T., Arshinov, M., Tans, P., Conway, T. J., Saito, M., Valsala, V., Oda, T., Andres, R. J., & Belikov, D. (2013). Carbon flux estimation for Siberia by inverse modeling constrained by aircraft and tower CO2 measurements <https://doi.org/10.1002/jgrd.50127>. *Journal of Geophysical Research: Atmospheres*, *118*(2), 1100–1122.

Sargent, M., Barrera, Y., Nehrkorn, T., Hutyra, L. R., Gately, C. K., Jones, T., McKain, K., Sweeney, C., Hegarty, J., Hardiman, B., Wang, J. A., & Wofsy, S. C. (2018). Anthropogenic and biogenic CO2 fluxes in the Boston urban region <https://doi.org/10.1073/pnas.1803715115>. *Proceedings of the National Academy of Sciences*, *115*(29), 7491–7496.

Sawa, Y., Machida, T., Matsueda, H., Niwa, Y., Tsuboi, K., Murayama, S., Morimoto, S., & Aoki, S. (2015). Seasonal changes of CO2, CH4, N2O, and SF6 in the upper troposphere/lower stratosphere over the Eurasian continent observed by commercial airliner <https://doi.org/10.1002/2014GL062734>. *Geophysical Research Letters*, *42*(6), 2001–2008.

Schmidt, M., Lopez, M., Kwok, C., Messager, C., Ramonet, M., Wastine, B., Vuillemin, C., Truong, F., Gal, B., Parmentier, E., Cloue, O., & Ciais, P. (2014). High-precision quasi-continuous atmospheric greenhouse gas measurements at Trainou tower (Orléans forest, France) <https://doi.org/10.5194/amt-7-2283-2014>. *Atmospheric Measurement Techniques*, *7*, 2283–2296.

Schmidt, U., & Khedim, A. (1991). In situ measurements of carbon dioxide in the winter Arctic vortex and at midlatitudes: An indicator of the "age" of stratospheric air <https://doi.org/10.1029/91GL00022>. *Geophysical Research Letters*, *18*(4), 763–766.

Schneider, M., Ertl, B., Tu, Q., Diekmann, C. J., Khosrawi, F., Röhling, A. N., Hase, F., Dubravica, D., García, O. E., Sepúlveda, E., Borsdorff, T., Landgraf, J., Lorente, A., Butz, A., Chen, H., Kivi, R., Laemmel, T., Ramonet, M., Crevoisier,

C., . . . Pollard, D. F. (2022). Synergetic use of IASI profile and TROPOMI total-column level 2 methane retrieval products <https://doi.org/10.5194/amt-15-4339-2022>. *Atmospheric Measurement Techniques*, *15*(14), 4339–4371.

Schuck, T. J., Brenninkmeijer, C. A. M., Slemr, F., Xueref-Rémy, I., & Zahn, A. (2009). Greenhouse gas analysis of air samples collected onboard the CARIBIC passenger aircraft. *Atmospheric Measurement Techniques*, *2*, 449–464.

Schwietzke, S., Harrison, M., Lauderdale, T., Branson, K., Conley, S., George, F. C., Jordan, D., Jersey, G. R., Zhang, C., Mairs, H. L., Pétron, G., & Schnell, R. C. (2019). Aerially guided leak detection and repair: A pilot field study for evaluating the potential of methane emission detection and cost-effectiveness <https://doi.org/10.1080/10962247.2018.1515123>. *Journal of the Air & Waste Management Association*, *69*(1), 71–88.

Sha, M. K., De Mazière, M., Notholt, J., Blumenstock, T., Chen, H., Dehn, A., Griffith, D. W. T., Hase, F., Heikkinen, P., Hermans, C., Hoffmann, A., Huebner, M., Jones, N., Kivi, R., Langerock, B., Petri, C., Scolas, F., Tu, Q., & Weidmann, D. (2020). Intercomparison of low- and high-resolution infrared spectrometers for ground-based solar remote sensing measurements of total column concentrations of CO2, CH4, and CO <https://doi.org/10.5194/amt-13-4791-2020>. *Atmospheric Measurement Techniques*, *13*(9), 4791–4839.

Stephens, B., Gurney, K., Tans, P., Sweeney, C., Peters, W., Bruhwiler, L., Ciais, P., Ramonet, M., Bousquet, P., Nakazawa, T., Aoki, S., Machida, T., Inoue, G., Vinnichenko, N., Lloyd, J., Jordan, A., Heimann, M., Shibistova, O., Langenfelds, R., . . . Denning, A. (2007). Weak northern and strong tropical land carbon uptake from vertical profiles of atmospheric CO2 <https://doi.org/10.1126/science.1137004>. *Science*, *316*(5832), 1732–1735.

Stuiver, M., & Polach, H. A. (2016). Discussion reporting of 14C data <https://doi.org/10.1017/S0033822200003672>. *Radiocarbon*, *19*(3), 355–363.

Stuiver, M., & Quay, P. D. (1981). Atmospheric14C changes resulting from fossil fuel CO2 release and cosmic ray flux variability <https://doi.org/10.1016/0012-821X(81)90040-6>. *Earth and Planetary Science Letters*, *53*(3), 349–362.

Suess, H. E. (1955). Radiocarbon concentration in modern wood. *Science*, *122*(3166), 415–417.

Sweeney, C., Karion, A., Wolter, S., Newberger, T., Guenther, D., Higgs, J. A., Andrews, A. E., Lang, P. M., Neff, D., Dlugokencky, E., Miller, J. B., Montzka, S. A., Miller, B. R., Masarie, K. A., Biraud, S. C., Novelli, P. C., Crotwell, M., Crotwell, A. M., Thoning, K., & Tans, P. P. (2015). Seasonal climatology of CO2 across North America from aircraft measurements in the NOAA/ESRL global greenhouse gas reference network <https://doi.org/10.1002/2014JD022591>. *Journal of Geophysical Research: Atmospheres*, *120*(10), 5155–5190.

Sweeney, C., McKain, K., Miller, B. R., & Michel, S. E. (2020). *ABoVE: Atmospheric gas concentrations from airborne flasks, Arctic-CAP, 2017* <https://doi.org/10.3334/ORNLDAAC/1717>. Dataset published by ORNL Distributed Active Archive Center.

Tans, P. P., Conway, T. J., & Nakazawa, T. (1989). Latitudinal distribution of the sources and sinks of atmospheric carbon dioxide derived from surface observations and an atmospheric transport model <https://doi.org/10.1029/JD094iD04p05151>. *Journal of Geophysical Research: Atmospheres*, *94*(D4), 5151–5172.

Tans, P. P., Fung, I. Y., & Takahashi, T. (1990). Observational constraints on the global atmospheric CO_2 budget. *Science*, *247*, 1431–1438.

Telegadas, K. (1971). *Seasonal atmospheric distribution and inventories of excess 14C from March 1955—July 1969* (pp. 1–2 in Report No. HASL-243). U.S. Atomic Energy Commission.

Thompson, R. L., Patra, P. K., Chevallier, F., Maksyutov, S., Law, R. M., Ziehn, T., van der Laan-Luijkx, I. T., Peters, W., Ganshin, A., Zhuravlev, R., Maki, T., Nakamura, T., Shirai, T., Ishizawa, M., Saeki, T., Machida, T., Poulter, B., Canadell, J. G., & Ciais, P. (2016). Top–down assessment of the Asian carbon budget since the mid 1990s <https://doi.org/10.1038/ncomms10724>. *Nature Communications*, *7*(1), 10724.

Thoning, K. W., Tans, P. P., & Komhyr, W. D. (1989). Atmospheric carbon dioxide at Mauna Loa observatory, 2, analysis of the NOAA GMCC data, 1974, 1985. *Journal of Geophysical Research*, *94*(D6), 8549–8565.

Tissandier, G. (1874). L'acide carbonique de l'air: dosages effectués à bord du ballon Le Zenith. *La Nature*, *79*, 331–334.

Tu, Q., Hase, F., Blumenstock, T., Kivi, R., Heikkinen, P., Sha, M. K., Raffalski, U., Landgraf, J., Lorente, A., Borsdorff, T., Chen, H., Dietrich, F., & Chen, J. (2020). Intercomparison of atmospheric CO2 and CH4 abundances on regional scales in boreal areas using Copernicus Atmosphere Monitoring Service (CAMS) analysis, COllaborative Carbon Column Observing Network (COCCON) spectrometers, and Sentinel-5 precursor satellite observations <https://doi.org/10.5194/amt-13-4751-2020>. *Atmospheric Measurement Techniques*, 13(9), 4751–4771.

Turnbull, J. C., Karion, A., Davis, K. J., Lauvaux, T., Miles, N. L., Richardson, S. J., Sweeney, C., McKain, K., Lehman, S. J., Gurney, K. R., Patarasuk, R., Liang, J., Shepson, P. B., Heimburger, A., Harvey, R., & Whetstone, J. (2019). Synthesis of urban CO2 emission estimates from multiple methods from the Indianapolis flux project (INFLUX) <https://doi.org/10.1021/acs.est.8b05552>. *Environmental Science & Technology*, *53*(1), 287–295.

Turnbull, J. C., Mikaloff Fletcher, S. E., Ansell, I., Brailsford, G. W., Moss, R. C., Norris, M. W., & Steinkamp, K. (2017). Sixty years of radiocarbon dioxide measurements at Wellington, New Zealand: 1954–2014 <https://doi.org/10.5194/acp-17-14771-2017>. *Atmospheric Chemistry and Physics*, *17*(23), 14771–14784.

Umezawa, T., Matsueda, H., Oda, T., Higuchi, K., Sawa, Y., Machida, T., Niwa, Y., & Maksyutov, S. (2020). Statistical characterization of urban CO2 emission signals observed by commercial airliner measurements <https://doi.org/10.1038/s41598-020-64769-9>. *Scientific Reports*, *10*(1), 7963.

Umezawa, T., Matsueda, H., Sawa, Y., Niwa, Y., Machida, T., & Zhou, L. (2018). Seasonal evaluation of tropospheric CO2 over the Asia-Pacific region observed by the CONTRAIL commercial airliner measurements <https://doi.org/10.5194/acp-18-14851-2018>. *Atmospheric Chemistry and Physics*, *18*(20), 14851–14866.

Vermeulen, A., Turnbull, J., Peuch, V.-H., Tarasova, O., & Volosciuk, C. (2020). *Response of carbon dioxide and air quality to the reduction in emissions due to the COVID-19 restrictions* (Report 69, 27–31). World Meteorological Organization.

Vermeulen, A. T., Hensen, A., Popa, M. E., van den Bulk, W. C. M., & Jongejan, P. A. C. (2011). Greenhouse gas observations from Cabauw Tall Tower (1992–2010) <https://doi.org/10.5194/amt-4-617-2011>. *Atmospheric Measurement Techniques*, *4*(3), 617–644.

Watson, A. J., Schuster, U., Shutler, J. D., Holding, T., Ashton, I. G. C., Landschützer, P., Woolf, D. K., & Goddijn-Murphy, L. (2020). Revised estimates of ocean-atmosphere CO2 flux are consistent with ocean carbon inventory <https://doi.org/10.1038/s41467-020-18203-3>. *Nature Communications*, *11*(1), 4422.

Weir, B., Crisp, D., O'Dell, C. W., Basu, S., Chatterjee, A., Kolassa, J., Oda, T., Pawson, S., Poulter, B., Zhang, Z., Ciais, P., Davis, S. J., Liu, Z., & Ott, L. E. (2021). Regional impacts of COVID-19 on carbon dioxide detected worldwide from space <https://doi.org/10.1126/sciadv.abf9415>. *Science Advances*, *7*(45), eabf9415.

Werle, P., Slemr, F., Maurer, K., Kormann, R., Mücke, R., & Jänker, B. (2002). Near- and mid-infrared laser-optical sensors for gas analysis <https://doi.org/10.1016/S0143-8166(01)00092-6>. *Optics and Lasers in Engineering*, *37*(2), 101–114.

World Data Centre for Greenhouse Gases. (2021). *WMO WDCGG data summary, Volume IV-Greenhouse and Related Gases* (Report 45). Japan Meteorological Agency in cooperation with World Meteorological Organization.

World Meteorological Organization. (2021). *The state of greenhouse gases in the atmosphere based on global observations through 2020* (Report 17 (WMO Greenhouse Gas Bulletin).

World Meteorological Organization. (2022). OSCAR <https://space.oscar.wmo.int/>.

World Meteorological Organization / International Atomic Energy Agency. (2020). *20th WMO/IAEA meeting on carbon dioxide, other greenhouse gases and related measurement techniques (GGMT-2019)*. Report 242 (A. Crotwell, H. Lee, & M. Steinbacher, Eds., published by World Meteorological Organization).

Wofsy, S. C., Harriss, R. C., & Kaplan, W. A. (1988). Carbon dioxide in the atmosphere over the Amazon Basin <https://doi.org/10.1029/JD093iD02p01377>. *Journal of Geophysical Research: Atmospheres*, *93*(D2), 1377–1387.

Wong, C. S., Chan, Y. H., Page, J. S., Smith, G. E., & Bellegay, R. D. (1993). Changes in equatorial CO2 flux and new production estimated from CO2 and nutrient levels in Pacific surface waters during the 1986/87 El Niño <https://doi.org/10.3402/tellusb.v45i1.15580>. *Tellus B: Chemical and Physical Meteorology*, *45*(1), 64–79.

Wunch, D., Toon, G. C., Blavier, J. F. L., Washenfelder, R. A., Notholt, J., Connor, B. J., Griffith, D. W. T., Sherlock, V., & Wennberg, P. O. (2011). The total carbon column observing network <https://doi.org/10.1098/rsta.2010.0240>. *Philosophical Transactions of the Royal Society A—Mathematical Physical and Engineering Sciences*, *369*(1943), 2087–2112.

Wunch, D., Toon, G. C., Sherlock, V., Deutscher, N. M., Liu, C., Feist, D. G., & Wennberg, P. O. (2015). *Documentation for the 2014 TCCON data release* <https://doi.org/10.14291/TCCON.GGG2014.DOCUMENTATION.R0/1221662> (CaltechDATA, Ed.). California Institute of Technology).

Wunch, D., Wennberg, P. O., Osterman, G., Fisher, B., Naylor, B., Roehl, C. M., O'Dell, C., Mandrake, L., Viatte, C., Kiel, M., Griffith, D. W. T., Deutscher, N. M., Velazco, V. A., Notholt, J., Warneke, T., Petri, C., De Maziere, M., Sha, M. K., Sussmann, R., . . . Eldering, A. (2017). Comparisons of the Orbiting Carbon Observatory-2 (OCO-2) XCO2 measurements with TCCON <https://doi.org/10.5194/amt-10-2209-2017>. *Atmospheric Measurement Techniques*, *10*(6), 2209–2238.

Yang, Z., Washenfelder, R. A., Keppel-Aleks, G., Krakauer, N. Y., Randerson, J. T., Tans, P. P., Sweeney, C., & Wennberg, P. O. (2007). New constraints on Northern Hemisphere growing season net flux. *Geophysical Research Letters*, *34*(12).

Yi, Y., Liu, Y., Cai, Z., Fang, S., Yang, D., Wang, Y., Liang, M., Yao, B., Ma, Q., & Wang, M. (2019). Measuring and comparing in-situ CO2 and CO profiles with satellite observations and model data <https://doi.org/10.1080/16742834.2019.1649974>. *Atmospheric and Oceanic Science Letters*, *12*(6), 444–450.

Yoshida, Y., Kikuchi, N., & Yokota, T. (2012). On-orbit radiometric calibration of SWIR bands of TANSO-FTS onboard GOSAT <https://doi.org/10.5194/amt-5-2515-2012>. *Atmospheric Measurement Techniques*, *5*(10), 2515–2523.

Zheng, B., Chevallier, F., Ciais, P., Broquet, G., Wang, Y., Lian, J., & Zhao, Y. (2020). Observing carbon dioxide emissions over China's cities and industrial areas with the Orbiting Carbon Observatory-2 <https://doi.org/10.5194/acp-20-8501-2020>. *Atmospheric Chemistry and Physics*, *20*(14), 8501–8510.

Notes

1. The quantity measured by in situ CO_2 analyzers is in atmospheric science expressed as molar fraction, corresponding to the number of molecules of carbon dioxide in a given number of molecules of air. In order to overcome the highly variable dilution by water vapor, the measurements are calculated as molar fraction in dry air. We, however, use here the term "concentration," which is more familiar in the general public, as well as the unit ppm (parts per million), corresponding to μmole of CO_2 per mole of dry air.